Meteoritics & Planetary Science 41, Nr 4, 581–606 (2006)
Abstract available online at http://meteoritics.org

Petrology and chemistry of MIL 03346 and its significance in understanding the petrogenesis of nakhlites on Mars

James M. D. DAY[1*], Lawrence A. TAYLOR[1], Christine FLOSS[2], and Harry Y. MCSWEEN JR.[1]

[1]Planetary Geosciences Institute, Department of Earth and Planetary Sciences, University of Tennessee, Knoxville, Tennessee 37996, USA
[2]Laboratory for Space Sciences, Washington University, St. Louis, Missouri 63130, USA
[*]Corresponding author. E-mail: jday13@utk.edu

(Received 03 March 2005; revision accepted 02 October 2005)

Abstract–Antarctic meteorite Miller Range (MIL) 03346 is a nakhlite composed of 79% clinopyroxene, ~1% olivine, and 20% vitrophyric intercumulus material. We have performed a petrological and geochemical study of MIL 03346, demonstrating a petrogenetic history similar to previously discovered nakhlites. Quantitative textural study of MIL 03346 indicates long (>1 × 10^1 yr) residence times for the cumulus augite, whereas the skeletal Fe-Ti oxide, fayalite, and sulfide in the vitrophyric intercumulus matrix suggest rapid cooling, probably as a lava flow. From the relatively high forsterite contents of olivine (up to Fo_{43}) compared with other nakhlites and compositions of augite cores ($Wo_{38–42}En_{35–40}Fs_{22–28}$) and their hedenbergite rims, we suggest that MIL 03346 is part of the same or a similar Martian cumulate-rich lava flow as other nakhlites. However, MIL 03346 has experienced less equilibration and faster cooling than other nakhlites discovered to date. Calculated trace element concentrations based upon modal abundances of MIL 03346 and its constituent minerals are identical to whole rock trace element abundances. Parental melts for augite have REE patterns that are approximately parallel with whole rock and intercumulus melt using experimentally defined partition coefficients. This parallelism reflects closed-system crystallization for MIL 03346, where the only significant petrogenetic process between formation of augite and eruption and emplacement of the nakhlite flow has been fractional crystallization. A model for the petrogenesis of MIL 03346 and the nakhlites (Nakhla, Governador Valadares, Lafayette, Yamato-000593, Northwest Africa (NWA) 817, NWA 998) would include: 1) partial melting and ascent of melt generated from a long-term LREE depleted mantle source, 2) crystallization of cumulus augite (± olivine, ± magnetite) in a shallow-level Martian magma chamber, 3) eruption of the crystal-laden nakhlite magma onto the surface of Mars, 4) cooling, crystal settling, overgrowth, and partial equilibration to different extents within the flow, 5) secondary alteration through hydrothermal processes, possibly immediately succeeding or during emplacement of the flow. This model might apply to single—or multiple—flow models for the nakhlites. Ultimately, MIL 03346 and the other nakhlites preserve a record of magmatic processes in volcanic rocks on Mars with analogous petrogenetic histories to pyroxene-rich terrestrial lava flows and to komatiites.

INTRODUCTION

The Shergotty-Nakhla-Chassigny (SNC) meteorites represent a suite of magmatic achondrites with a range of mafic to ultramafic compositions, including basalts and basaltic lherzolites (shergottites), clinopyroxenites (nakhlites), orthopyroxenite Allan Hills (ALH) 84001, and dunites (Chassigny and NWA 2737). The SNC meteorites share common stable and noble gas isotope signatures and major and trace element traits that distinguish them from other differentiated meteorites (e.g., McSween 1994; Clayton and Mayeda 1996; McSween and Treiman 1998). The chemical and petrological similarities of these meteorites, along with shock-implanted noble gas isotopic compositions that are within error of the Martian atmospheric composition measured by the Viking landers, indicate that the SNC meteorites probably originate from Mars (e.g., Bogard and Johnson 1983).

At present, there are in excess of 30 SNC meteorites in the terrestrial collections, excluding paired meteorites from localized falls. Of these, shergottites represent the most abundant type of SNC meteorites (~70% of all finds), with the

least abundant types represented by ALH 84001 (orthopyroxenite) and Chassigny and NWA 2737 (dunites). Finds for the second most abundant SNC meteorite subgroup, the nakhlites, have more than doubled since the year 2000 (from 3 to 7 nakhlite meteorites), and it is one of these nakhlites, Miller Range (MIL) 03346, that is described in detail here. We present a quantitative petrological and geochemical study for this 715 g stone, which is only the second nakhlite discovered in the Antarctic. Although similar to other nakhlites, the more fractionated nature of MIL 03346 intercumulus matrix and lack of equilibration of mineral phases relative to other nakhlites leads us to suggest modifications to an igneous cumulate model first proposed by Bunch and Reid (1975) for the petrogenesis of nakhlites.

SAMPLES AND ANALYTICAL METHODS

Textural Analysis

Two polished thin sections of MIL 03346 (111 and 118) were examined to study their petrographic characteristics. Quantitative textural analysis was performed to determine porosity (percentage melt), XY grain center coordinates, orientations, and lengths (long and short axis) following the protocols of Jerram et al. (2003). This technique involves the identification and outlining of crystals and conversion of the monomineralic texture to a digital bitmap image, after which each crystal is identified individually prior to processing using image analysis software (e.g., Fig. 1). The resultant quantitative textural information is used to provide crystal size distribution (CSD) and spatial distribution patterns (SDP). Digitized images were processed using freeware (Image Tool), and 3-D crystal dimensions were predicted using the method of Morgan and Jerram (Forthcoming). The CSD patterns were calculated using CSD correction software, version 1.36 (Higgins 2000) and R values were calculated according to the technique of Jerram et al. (1996) using Big-R software (M. J. Higgins, unpublished data).

Mineral Chemical Analysis

Electron microprobe analyses were performed on two polished sections of MIL 03346. Mineral modes were determined using Feature Scan software with an Oxford Instrument energy dispersive spectrometer (EDS) according to the procedure of Taylor et al. (1996). The EDS unit is part of the automated CAMECA SX-50 electron microprobe analyzer (EMPA) at the University of Tennessee. Mineral compositions were determined in wavelength dispersive spectral (WDS) mode on the EMPA using an accelerating potential of 15 KeV, a 20 nA beam current (6 nA for glasses), 1 μm beam size (5–10 μm for glasses), peak and background counting times of 20–30 s, and standard ZAF (PAP) correction procedures. A combination of natural and synthetic standards were used for calibration and were measured periodically within analytical sessions to ensure data quality. Drift was within counting error throughout every analytical session. Detection limits (3σ above background) are typically <0.03 for SiO_2, TiO_2, Al_2O_3, MgO, CaO, Na_2O, K_2O and Cl, and <0.05–0.1 for all other oxides and elements listed.

Concentrations of the REE and other trace elements were determined on MIL 03346, 111 using the modified Cameca ims 3f ion microprobe at Washington University according to techniques described by Zinner and Crozaz (1986a). Analyses were made using an O^- primary beam and energy filtering at low mass resolution to remove complex molecular interferences. The resulting mass spectrum is deconvolved in the mass ranges K-Ca-Sc-Ti, Rb-Sr-Y-Zr, and Ba-REE to remove simple molecular interferences that are not eliminated with energy filtering (Alexander 1994; Hsu 1995). Sensitivity factors for the REE are from Zinner and Crozaz (1986b) and those for other elements are from Hsu (1995) and are listed in Table 1 of Floss et al. (1998). Absolute concentrations are determined using sensitivity factors relative to Si, with SiO_2 concentrations determined by EMPA of the specific grains chosen for ion probe analysis. Reported errors are 1σ and are due to counting statistics only.

Whole Rock Major and Trace Element Analyses

A 2 g sub-sample of MIL 03346 (45) was provided by the Meteorite Working Group for whole rock geochemical studies. The sample was crushed in an agate pestle and mortar under class 100 airflow. Major element compositions were measured on ~10 mg of whole rock powder that was fused into a glass bead on a Mo-strip heater, in a nitrogen atmosphere. Fused bead major element concentrations were analyzed by EMPA with protocols for glass analyses. The average of 20 spot analyses is reported on a Mo-free basis. Trace element concentrations were measured on a 20 mg aliquot using an ELAN 6000 inductively coupled plasma-mass spectrometer (ICP-MS) at the University of Durham following the procedure of Ottley et al. (2003). The remaining sample mass is being used for ongoing isotope studies of this meteorite.

RESULTS

Quantitative Petrography and Textures

MIL 03346 is an unbrecciated clinopyroxenite with cumulus augite and rare cumulus olivine, set in a vitrophyric matrix containing skeletal Fe-Ti oxides, sulfides, secondary alteration phases, and sulfide-Fe-Ti oxide-fayalite "filaments" (Figs. 1 and 2). Results of X-ray modal analysis for MIL 03346 are presented with previously published data for the other nakhlites in Table 1. Modal analysis for MIL 03346 was performed on a polished surface of 110 mm^2. The

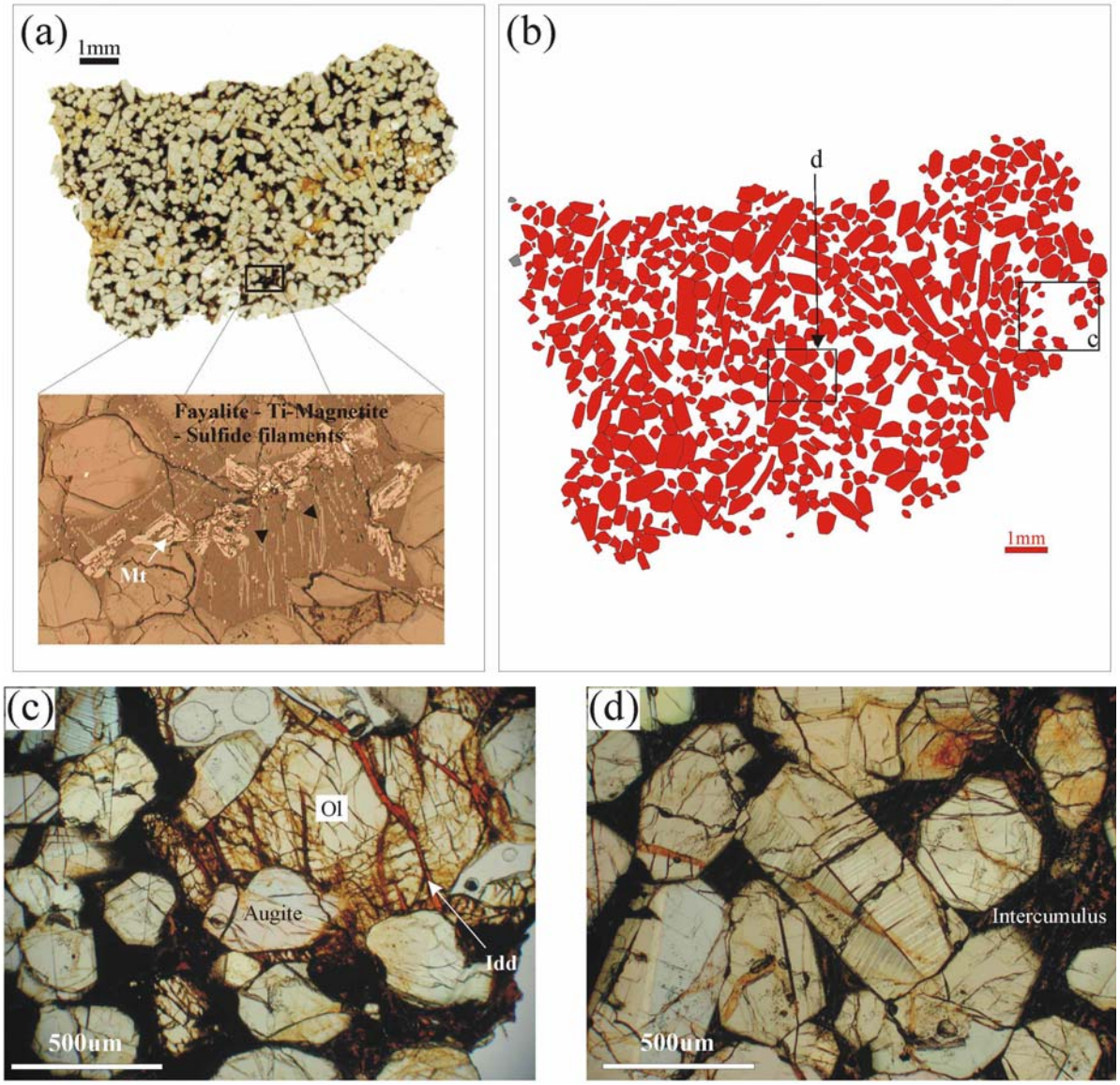

Fig. 1. a) A plain-polarized light photomicrograph of polished section MIL 03346, 111 illustrating the cumulus augite and vitrophyric intercumulus matrix. Inset reflected light photomicrograph illustrating intercumulus Ti magnetite and filaments of fayalite, Ti magnetite, and sulfide—textures typical of fast cooling. b) A digitally edited image of augite cumulate MIL 03346, with locations of photomicrographs (c) and (d). c) A plain-polarized light photomicrograph of olivine partially enclosing augite. Iddingsite (Idd) occupies fractures within the olivine. d) A plain-polarized light photomicrograph of chevron twined shock lamellae in a cumulus augite and the touching framework of cumulus augite crystals.

sample is composed of 79% clinopyroxene, 1% olivine (varies to ≤4% for some sections, e.g., McKay and Schwandt 2005; Mikouchi et al. 2005) and 20% vitrophyric intercumulus matrix, containing 1% opaque phases.

Evaluation of nakhlite modes shows that Nakhla, Lafayette, Governador Valadares, Yamato-000593/749/802 (hereafter referred to as Y-000593), NWA 817, and NWA 998 all contain more olivine than MIL 03346. Miller Range 03346, NWA 817, and NWA 998 have slightly higher proportions of intercumulus material than the four other nakhlites. Based on their modal mineralogy, the nakhlites can be subdivided into crude groupings. The first group includes those with higher proportions of intercumulus vitrophyric groundmass (MIL 03346 and NWA 817) and the second group includes those with lower proportions of intercumulus crystalline groundmass (Nakhla, Lafayette, Governador Valadares, Y-000593, NWA 998).

Miller Range 03346 has the largest average crystal size population of any nakhlite (Table 2), with clinopyroxenes ranging in length from 0.2–2.5 mm, with average dimensions of 0.43 × 0.26 mm; Stopar et al. (2005) determined a similar average width for pyroxene grains for MIL 03346 of 0.27 mm. The clinopyroxenes have Fe-enriched rims that are approximately 10 μm in thickness (~50 μm where crystal

Table 1. Modal analysis of MIL 03346 and comparison with other nakhlite modal percentages.

	MIL 03346[a]	NWA 998[b]	NWA 817[c]	Yamato-593[d]	Gov. Vala.[e]	Lafayette[e]	Nakhla[e]
Pyroxene	78.4	70	69	76.7	81.2	73.5	80.8
Augite	67.5	68	69	76.7	81.2	73.5	80.8
Ferro-pyroxene	10.8	–	–	–	–	–	–
Pigeonite	0.2	–	–	–	–	–	–
Orthopyroxene	<0.1	2	–	–	–	–	–
Olivine	1.1	10	12.5	12.2	8.9	16.7	10.8
Fayalite	1.1		–	–	–	–	–
Forsterite	0.03 [0.5]		–	–	–	–	–
Intercumulus matrix	19.8	19	18.5	11.1	9.8	9.8	8.4
Na-rich albite glass	18.5	–	–	–	–	–	–
Ti magnetite	1.0	–	1	0.6	–	–	–
Plagioclase	0.1						
Sulfide	0.04	–	–	–	–	–	–
Phosphate	0.01	–	–	–	–	–	–
K-rich phase	0.17	–	–	–	–	–	–
Alteration	0.24						
Iddingsite	0.24	–	–	–	–	–	–

Data bins defined according to: augite = 6–20% Mg, 47–62% Si, 19–40% Ca, ferro-pyroxene = 0–7% Mg, 45–62% Si, 17–32% Ca, 10–34% Fe, pigeonite = 49–66% Si, 4–12% Ca, 10–46% Fe, 0–6% Al, fayalite = 0–7% Mg, 30–45% Si, 0–2% Ca, 0–4% Al, olivine = 7–60% Mg, 30–45% Si, 0–2% Ca and Al, iddingsite = 45–65% Si, 27–60% Fe (other classifications available from the corresponding author upon request).
Model percentage data from: [a]This study; [b]Treiman 2005; [c]Sautter et al. 2002; [d]Imae et al. 2003; [e]Lentz et al. 1999.

faces are not perpendicular to the section plane) and vary from subhedral to euhedral tabular or equant morphologies. Some of the large clinopyroxenes exhibit well-developed "chevron" twinning and planar deformation features (Fig. 1d).

Large (0.1–1.5 mm), rare olivines are pervasively altered and poikilitically enclose pyroxenes without Fe-enriched rims (Figs. 1c and 3b). Based on this texture, the olivines appear to have crystallized after augite, in contrast to Nakhla, where the opposite sequence has been observed (e.g., Harvey and McSween 1992a, 1992b). The olivines are anhedral and lack the dark lamellar symplecite exsolution (augite-magnetite intergrowths) observed in Nakhla or Governador Valadares (e.g., Greshake et al. 2000). Modal analysis of MIL 03346 further subdivides the major cumulus and intercumulus phases (Table 1), based upon Mg# for olivine. Most of the olivine in MIL 03346 is intercumulus fayalite ($\geq Fa_{90}$) whereas more forsteritic ($\leq Fo_{43}$), larger, poikilitic olivine grains represent from 0.03% to a maximum of 0.5% of the polished section surface areas of MIL 03346.

The vitrophyric intercumulus matrix of MIL 03346 lacks feldspar as well as large phosphate-rich crystalline phases, and is dominantly composed of a Na-rich, non-stoichiometric albitic glass. The intercumulus matrix of MIL 03346 is texturally and mineralogically more diverse than other nakhlites (Figs. 1 and 2; Table 1). Titanomagnetite octahedral, cruciform and complex skeletal growth morphologies occur in the intercumulus matrix (Fig. 3c); such features commonly occur in quenched terrestrial basaltic flows (Haggerty 1976). These Ti-magnetite morphologies have only previously been reported in the nakhlite NWA 817 (Sautter et al. 2002) and in the fusion crust of Lafayette (Boctor et al. 1976). The intercumulus matrix also contains large angular or blocky opaque phases, commonly associated with complex alteration zones, as well as sulfide droplets and "filaments" composed of sulfide, Fe-Ti oxide, and fayalite (Figs. 1 and 2). The Fe-Ti oxides are "spongy" and contain fine exsolved spindles of ilmenite, although these are more poorly developed than those exhibited in NWA 817.

The predominant alteration product occurs as a reddish-orange mineral that is smeared in portions of the thin sections when viewed in plane-polarized light. Its occurrence in olivine is widespread, where it is generally found along pre-existing fracture planes (Figs. 1 and 3). Similar alteration phases have been recognized in all other nakhlites and have variously been referred to as iddingsite (e.g., Prior 1912; Bunch and Reid 1975; Bridges and Grady 2000), serpentine (Irving et al. 2002), or smectite clays (Treiman et al. 1993). This alteration assemblage probably represents a sub-micrometer mixture of smectite clay, iron oxyhydroxides, and salt minerals (Treiman 2005).

Crystal Size Distribution

Crystal size distribution (CSD) analysis is a well-established and statistically viable tool for the quantitative petrographic analysis of igneous and metamorphic rocks (Marsh 1998; Higgins 2000). Quantification of the crystal population density of a phase at given size intervals can be used, via a CSD plot, to gain important information about the growth history of crystal populations. CSD theory is based on the concept that the crystallizing system achieves steady-state

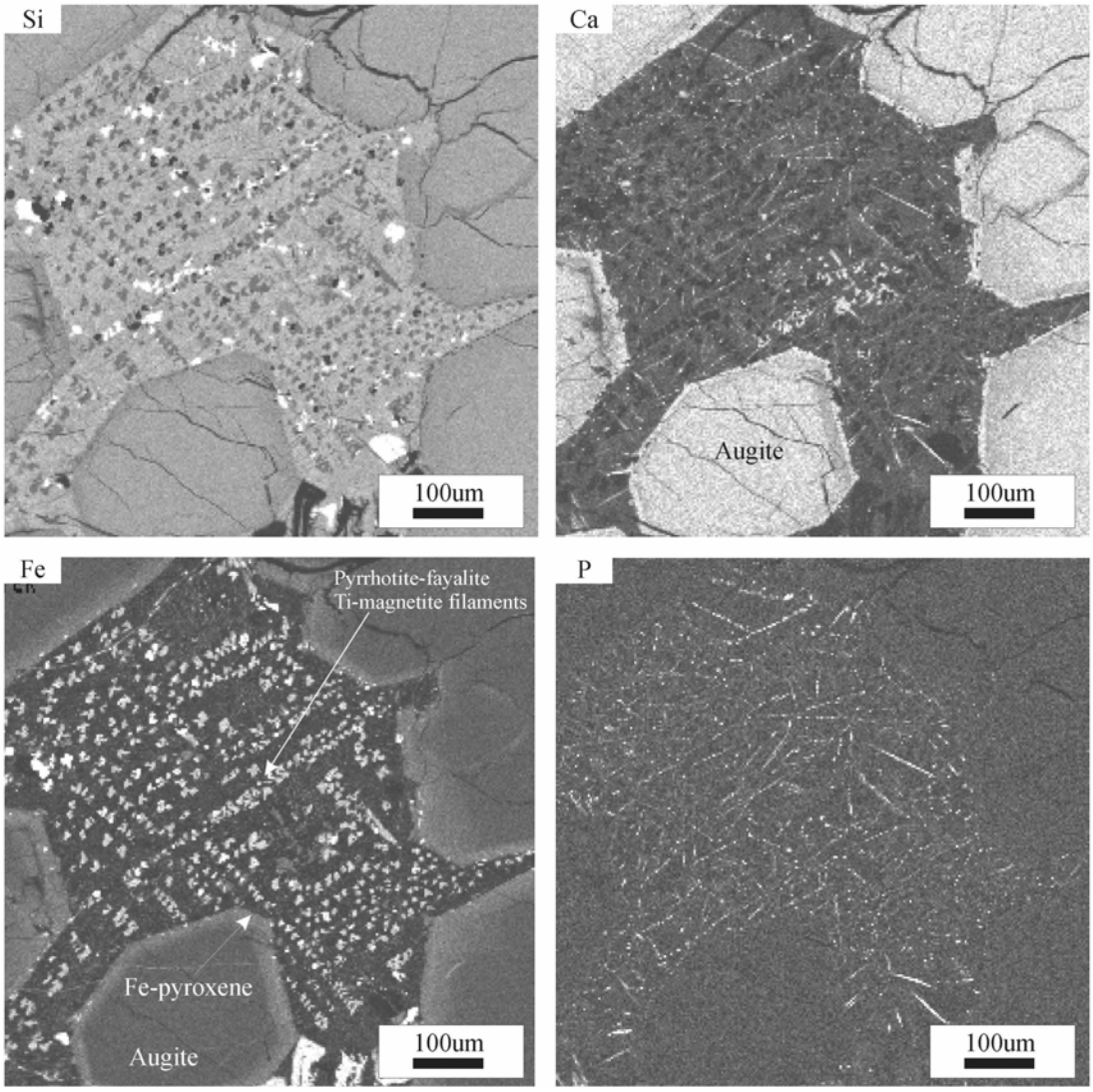

Fig. 2. Silica (Si), calcium (Ca), iron (Fe), and phosphorous (P) X-ray maps of the vitrophyric intercumulus matrix of MIL 03346 showing Si-, Ca-, Fe-, and P-rich phases within the intercumulus matrix of MIL 03346. The Fe-rich filaments have a knitted patchwork-like texture, while blades of phosphate occur throughout. Also, note the zonation of pyroxene crystals representing the change from augite cores to hedenbergite rims.

conditions whereby continuous nucleation and growth produce a skewed distribution of grain sizes, thus generating a negative linear plot in population density-crystal size space. The population density (n) of the articles in questions (crystals, vesicles, etc.) is linked to their size (L), whereas growth rates (G), residence time (τ) and final nucleation density (n_0) are constant for an individual CSD such that:

$$n = n_0 \exp(-L/G\tau) \quad (1)$$

This theoretical relationship is only valid in a steady-state open system. CSDs are often not straight lines, but individual straight portions of the CSD plot may be regressed. Linear regression analysis of the CSD curve provides a measure of growth rate/residence time (slope) and nucleation density (intercept). In addition, the shape of the CSD curve can reveal the operation of different processes during crystallization of magma batches (Marsh 1998).

Results of CSD analysis are presented in Table 2 and Fig. 4. The grain aspect ratios for the two sections analyzed, based upon 3-D crystal dimension predictions (Morgan and Jerram, Forthcoming) and employed for CSD correction, were 1:1.2:1.6 and 1:1.1:1.5 for MIL 03346, 111 and 118, respectively. On first inspection, the measured length and width CSDs show a similar log-linear relationship, differing only slightly in pattern morphology and population density, as expected for the abundance of crystals in thin sections. This relationship implies that steady-state nucleation and growth were important processes in the formation of the augite population.

Table 2. Crystal size and spatial distribution quantitative data for nakhlites.

Sample	Orientation	Area (mm^2)	No. of grains	Average dimensions	Slope (mm^{-1})	Intercept	R value	T $(10^{-10})^a$	T $(10^{-8})^a$
MIL 03346, 111	Length	110	596	0.43	−4.0	5.01	1.42	79	0.8
	Width			0.26	−5.8	6.08		55	0.6
MIL 03346, 118	Length	109	545	0.40	−3.7	4.58	1.35	86	0.9
	Width			0.25	−6.1	5.88		52	0.5
Nakhla (USNM)	Width	115	1024	0.24	−18.9	10.5	–	17	0.2
Nakhla (AMNH)	Width	134	1268	0.22	−22.2	11.3	–	14	0.1
Lafayette (USNM)	Width	56	810	0.19	−20.5	10.4	–	15	0.2
Lafayette (ASU)	Width	52	680	0.18	−20.5	10.2	–	15	0.2
GV (BM)	Width	88	852	0.20	−27.4	12.5	–	12	0.1

[a]Using a range of growth rates (numbers in parentheses are in mm/s, with *T* in Earth years) from experimental and natural systems (e.g., Cashman and Marsh 1988).

Data for Nakhla, Lafayette, and Governador Valadares (GV) from Lentz et al. 1999; note R-values for these nakhlites are not published.

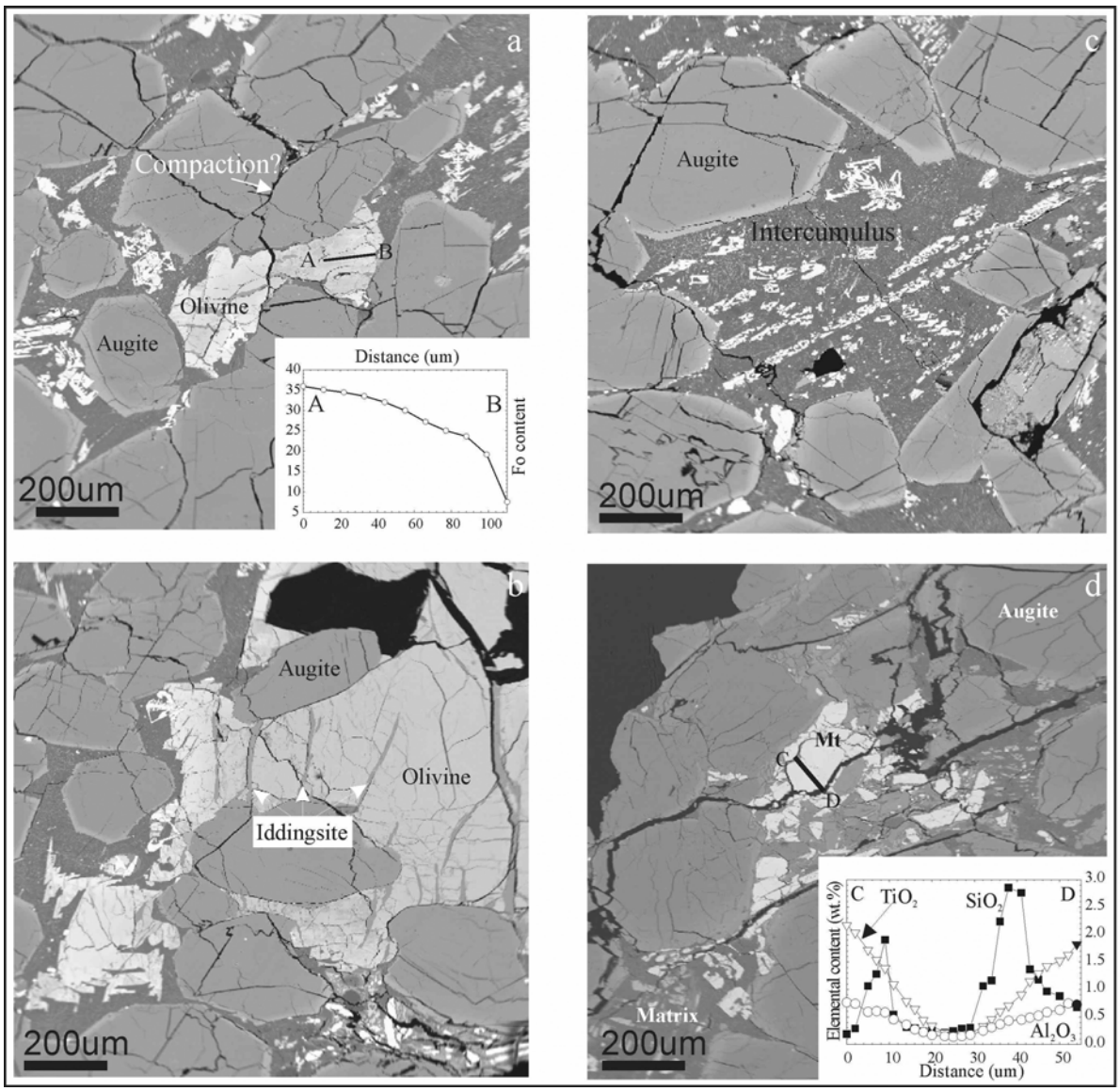

Fig. 3. Backscattered electron images of a) and b) cumulus olivine and augite showing the poikilitic nature of some olivines, c) skeletal and filament morphologies of Ti magnetite and fayalite-Ti magnetite-sulfide assemblages, and d) rhombohedral magnetite (Mt). EMPA traverses across cumulus olivine and magnetite illustrate zonation of these phases where they are in contact with the intercumulus matrix.

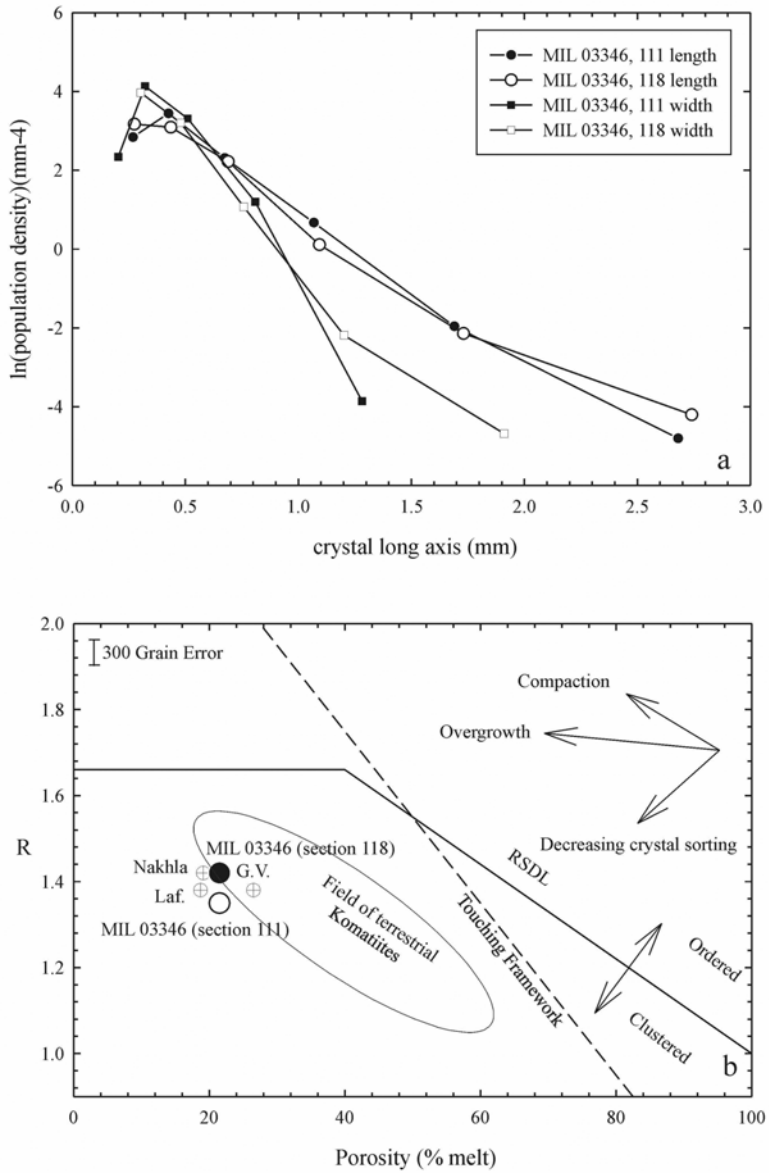

Fig. 4. a) CSD analyses of polished sections MIL 03346 111 and 118 analyzed for both crystal length and width and b) cluster analysis diagram (after Jerram et al. 2003) for Nakhla, Lafayette (Laf.) and Governador Valadares (G.V.) (Lentz et al. 1999), with new data for MIL 03346. This relationship suggests that nakhlites possess poorly sorted, clustered crystal frameworks.

Linear plots of population density versus crystal size for nakhlite augites have slopes that are equal to $-1/(G\tau)$ (Marsh 1998). This relationship means that residence times for augite crystal clusters can be calculated if an augite growth rate is estimated. Calculation of this residence time using typically estimated growth rates for silicate minerals in basaltic melts of $1–5 \times 10^{-10}$ mm/s (Cashman and Marsh 1988; Jerram et al. 2003) give residence times for MIL 03346 augites in the range of 1×10^2 to 1×10^3 years (Table 2). These calculated residence times are similar to estimates for Nakhla, Lafayette, and Governador Valadares (1×10^2 years) using identical growth rates and maximum width measurements. It should be noted that on this basis, if Lentz et al. (1999) used long-axis data, the residence times of their crystals would be longer. Employing the growth rates used by Lentz et al. (1999) from the study of McCoy and Lofgren (1999), who studied growth rates in shergottite pyroxenes at 1 atm and assumed the resultant crystals formed in situ, give considerably shorter residence times of $\leq 1 \times 10^1$ years.

The discrepancy in the slope of the crystal long-axis versus population density (Fig. 4) between MIL 03346 studied here and other nakhlites studied by Lentz et al. (1999), indicates a difference in average width crystal size and crystal population. For example, Lentz et al. (1999) measured, on average, 11.1 grains/mm^2 for their nakhlites, whereas we have measured, on average, 5.2 grains/mm^2. This may represent: a)

Table 3. Representative EMPA data for pyroxene in MIL 03346.

wt%	Cumulus pyroxene						Intercumulus pyroxene	
	Pyroxene #1			Pyroxene #2				
	Core	Midpoint	Rim	Core	Midpoint	Rim		
SiO_2	52.3	49.6	44.2	52.2	48.9	47.0	45.7	47.8
TiO_2	0.26	0.51	1.75	0.27	0.63	0.86	0.29	0.41
Al_2O_3	0.87	1.79	5.64	0.86	1.80	2.53	3.35	1.35
Cr_2O_3	0.40	0.08	<0.05	0.32	<0.05	<0.05	<0.05	<0.05
MgO	13.0	9.08	2.07	13.2	7.25	3.86	2.35	4.87
CaO	19.3	17.60	19.3	19.3	16.7	15.7	10.2	13.0
MnO	0.40	0.55	0.54	0.42	0.67	0.76	0.91	0.84
FeO	13.2	20.5	25.9	13.4	23.5	28.8	36.1	31.6
Na_2O	0.25	0.30	0.37	0.22	0.29	0.22	0.19	0.21
Total	100.0	100.1	99.7	100.1	99.8	99.8	99.2	100.1
Fs	22	35	48	22	41	52	68	56
En	38	27	7	38	22	12	7	15
Wo	40	38	46	40	37	36	25	29

a discrepancy due to the different techniques employed (here using tracing and digitization technique of Higgins (1994; 2000) and Jerram et al. (2003) versus Lentz et al. (1999) who used digital imaging or X-ray maps for CSD analysis); or b) fundamental differences in crystal size, overgrowth, and post-crystallization processes controlling crystal morphologies in the nakhlites. The latter alternative can be understood quantitatively using spatial distribution patterns.

Spatial Distribution Pattern

Spatial distribution pattern (SDP) analysis quantifies the arrangement of spatially related crystal constituents with R values (Jerram et al. 1996), thereby distinguishing touching crystal frameworks and providing a method to quantify the packing arrangement of crystals in the rock. The *R* value can be used to determine the clustering of touching crystal frameworks by comparison with the distribution of randomly packed spheres (Jerram et al. 1996; Jerram et al. 2003). The R value is defined as:

$$R = (2\sqrt{\rho\Sigma}r)/N \quad (2)$$

where ρ is the density of the observed distribution, *r* is the nearest neighbor distance, and *N* is the total number of individuals measured. Crystal clusters are common, if not ubiquitous, in phenocryst populations and may represent the building blocks of all igneous rocks (e.g., Jerram et al. 2003). Results of SDP analysis are presented in Table 2 and Fig. 4. The SDP analyses of MIL 03346 lie well within the "clustered" touching framework field, with both sections being within error of one another and data for Nakhla, Governador Valadares, and Lafayette. This statistical clustering of grains suggests that grains did not form and accumulate as individuals, but rather formed via poor sorting during accumulation as clumps. In this respect, the nakhlites are similar to most terrestrial komatiitic and basaltic lava flows analyzed with the SDP technique (e.g., Jerram et al. 2003).

Major-Element Mineral Chemistry

Pyroxene cores are augite (Mg# = $Mg/(Fe^{2+} + Mg)$ = 0.64–0.61) with a limited range of compositions ($Wo_{38–42}En_{35–40}Fs_{22–28}$) (Table 3; Fig. 5) that are nearly identical to those measured in other nakhlites (e.g., Treiman 2005). There is a sharp zonation on the rims of augite grains to hedenbergite compositions when they are in contact with the intercumulus matrix ($Wo_{25}En_8Fs_{67}$ to $Wo_{45}En_4Fs_{51}$) (Fig. 5). Orthogonal EMPA traverses performed across chevron twinning in augite crystals are compositionally homogeneous ($Wo_{38–42}En_{35–40}Fs_{22–28}$), indicating that crystal deformation processes, most probably impact-induced shock and not exsolution, are responsible for these features (e.g., Fig. 1d). Augite cores have relatively low Al, Ti, and Na concentrations ($Al_2O_3 = 0.9 \pm 0.1$ wt%; $TiO_2 = 0.3 \pm 0.1$ wt%; $Na_2O = 0.3 \pm 0.1$ wt%) with respect to terrestrial pyroxenes, consistent with crystallization at low pressure (Harvey and McSween 1992a). The pyroxene rims are more enriched in Al_2O_3 (8 wt%), TiO_2 (2.7 wt%) and Na_2O (0.4 wt%) than the cores. In addition to Fe-rich pyroxene rims, a few Fe-enriched intercumulus pyroxenes are also present within the intercumulus matrix of MIL 03346 (Fig. 5).

Olivine compositions range from Fo_{43} to Fo_4 (Table 4 and Fig. 5). The olivines can be separated into 1) rare (3 found in ~2.2 cm^2 area), large, poikilitic, relatively forsteritic olivines (Figs. 1c and 3) that have Fe-enriched rims and 2) fayalite filaments occurring with pyrrhotite and titano-magnetite in the intercumulus matrix (Fig. 3). The core compositions of the large poikilitic olivines are more forsteritic than those of Nakhla, Governador Valadares, Lafayette, NWA 998, or Y-000593 ($Fo_{33–38}$), but are similar to those found in NWA 817 (Fo_{41}). The rare, large cumulus olivines are zoned over distances of 50–100 μm (Fig. 3a). CaO contents are high (≥0.6 wt%) in the olivine cores and decrease to 0.15 wt% in the crystal margins. These values are consistent with crystallization at low pressure from a basaltic

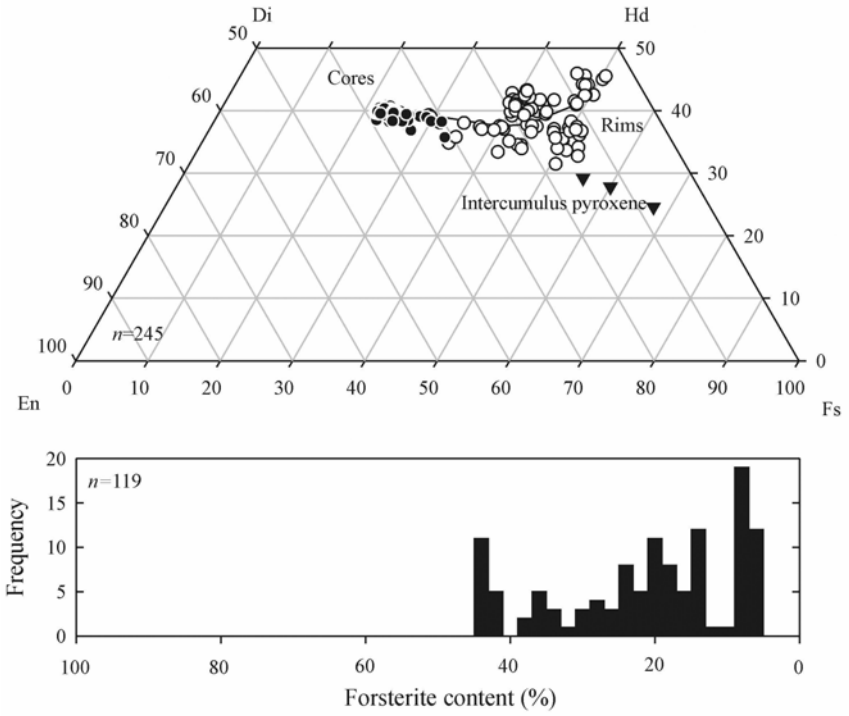

Fig. 5. Pyroxene and olivine compositions for MIL 03346. Shown on the quadrilateral are core-to-rim variations of pyroxenes and the presence of "intercumulus pyroxenes" that are reminiscent of pyroxenes found in the intercumulus matrix of other nakhlites (e.g., Treiman 2005). The dominant composition of the olivine population in MIL 03346 is fayalitic.

melt composition. The fayalite filaments have low CaO (≤0.05 wt%).

Magnetites in MIL 03346 span a wide range of compositions (Table 5) (Fe^{2+}/Fe^{3+} determined from 8-oxygen stoichiometry; Usp_0-Mt_{100} to Usp_{71}-Mt_{29}; Fig 6., which is greater than those previously reported for Nakhla (Usp_{39}-Mt_{61} to Usp_{45}-Mt_{55}) (McSween and Treiman 1998), or for NWA 817 (Usp_{31}-Mt_{69} to Usp_{44}-Mt_{56}) (Sautter et al. 2002), the closest petrographic analogue to MIL 03346. Low-Ti magnetite forms as distinct angular or blocky rhombohedral crystals associated with areas of secondary alteration and pseudo-brecciation (Fig. 3d). These crystals are very different from the Ti-magnetites (Usp_{65}-Mt_{35} to Usp_{71}-Mt_{29}) with the skeletal morphologies in the vitrophyric intercumulus matrix. One magnetite has a distinct SiO_2-rich rim at the junction between high (>1 wt%) and low (<1 wt%) TiO_2, possibly indicating later overgrowth (Fig. 3). No pure ilmenite compositions were measured, but Ti-rich lamellae exist within some of the skeletal Ti-magnetite crystals.

The intercumulus matrix is dominated by sodic glass with K-, P-, and Si-rich fractions (Table 6; Fig. 7). Previous studies have referred to this material as mesostasis, literally meaning middle standing or interstitial. However, we refrain from this terminology because of the inherent association it implies (as a direct in situ fractionation product) with the cumulus crystals in nakhlites. Efforts were made to analyze only the pure phases of the intercumulus matrix, using X-ray maps and backscattered electron (BSE) images for guidance. Unlike other nakhlites, MIL 03346 contains only limited, small (≤5 μm) feldspar grains and plagioclase composition melt inclusions, but Fe-rich albitic glass is present. These glass compositions plot in the transitional alkaline fields on an IUGS total alkali versus silica plot for terrestrial igneous rocks, and are similar to the compositions of some melt inclusions in nakhlites (Fig. 7). Within the glass, there are pockets with high P_2O_5, K_2O and impure silica (90 to 98 wt% SiO_2) (Fig. 2).

The vitrophyric matrix is populated by skeletal Ti-magnetite crystals, magmatic sulfide blebs (≤300 μm) and "filaments" of fayalite, Ti magnetite, and sulfides. The sulfides that occur within the intercumulus matrix are all pyrrhotite with (Fe + Ni + Co)/S atomic ratios ~0.89 (Table 5); fayalites range between $Fo_{4–8}$ (Table 4). Larger, euhedral to sub-rounded pyrrhotites also exist within the matrix and are pervasively altered. Morphologically, these large pyrrhotites differ from intercumulus matrix pyrrhotites within fayalite-Ti magnetite-sulfide associations, but both have similar bulk chemical compositions (Table 5). X-ray dispersive maps of the intercumulus matrix reveal the complex interplay of phases, with Si- and K-rich zones and more defined acicular P-rich needles (Fig. 2).

There are a number of alteration phases in MIL 03346, most of which are iron-rich hydroxysilicates (Table 7) with up to 14 wt% H_2O (as OH groups) and oxide components, apart from SiO_2, FeO and MgO, that are below 1 wt%. These iron-rich hydroxylsilicates are generally associated with the

Table 4. Representative EMPA data for olivine in MIL 03346.

wt%	Poikilitic olivine				Intercumulus fayalite		
	Olivine #1	Olivine #2					
	Core	Core	Midpoint	Rim			
SiO_2	34.2	34.1	32.7	32.1	29.7	29.9	29.8
TiO_2	0.03	<0.03	<0.03	<0.03	0.14	0.17	0.12
Al_2O_3	<0.03	<0.03	0.03	<0.03	0.04	<0.03	0.06
Cr_2O_3	–	<0.05	–	–	<0.05	<0.05	–
NiO	<0.05	–	<0.05	–	–	–	<0.05
MgO	19.0	19.1	13.8	10.4	1.85	2.40	1.72
CaO	0.56	0.54	0.53	0.55	0.19	0.16	0.19
MnO	0.93	0.99	1.06	1.16	1.79	2.02	1.69
FeO	45.7	45.8	52.2	55.5	65.6	64.8	65.6
Na_2O	–	<0.03	–	–	–	–	–
Total	100.4	100.6	100.4	99.7	99.3	99.5	99.1
Fo	43	43	32	25	5	6	4
Fa	57	57	68	75	95	94	96

Table 5. Representative EMPA data for Fe-Ti oxides and sulfides in MIL 03346.

wt%	Mt	TM	TM	TM	TM	TM		Pyrrhotite	Pyrrhotite	Pyrrhotite
Morphology	Rhom.	Oct. L	Comp.	Oct.	Cruci.	Oct. L		Inter.	Inter.	Xeno.
SiO_2	0.21	0.24	0.74	0.30	0.30	0.24	S	40.4	41.1	38.4
TiO_2	0.55	9.46	13.65	15.39	16.31	22.55	Fe	61.0	59.4	60.6
Al_2O_3	0.28	3.47	2.59	3.06	2.84	2.31	Co	0.08	<0.05	0.08
Cr_2O_3	0.05	<0.05	<0.05	<0.05	<0.05	<0.05	Ni	<0.05	<0.05	0.05
V_2O_3	<0.05	0.38	0.40	0.37	0.42	0.26	Si	<0.03	0.07	0.03
Fe_2O_3	67.2	45.0	36.2	33.6	31.3	19.7	Ca	0.03	0.04	0.05
FeO	31.7	39.8	43.9	45.1	45.5	50.8	P	<0.03	<0.03	–
MnO	0.11	0.45	0.46	0.55	0.58	0.66	Al	–	–	<0.03
MgO	0.05	0.11	0.11	0.09	0.12	0.14	Ti	–	–	<0.03
CaO	<0.03	<0.03	0.03	<0.03	0.06	0.06	Total	101.5	100.7	100.7
ZnO	<0.05	<0.05	<0.05	<0.05	<0.05	<0.05				
Total	100.2	99.0	98.1	98.4	97.3	96.7				
Molar%										
Usp.	1	28	39	45	47	65				
Mt.	99	73	61	55	53	36				

Mt = magnetite; TM = titanomagnetite; Rhom. = rhombic; Cruci. = cruciform; Oct. = octahedral; Comp. = complex; L = exsolved lamellae; Usp. = ulvöspinel (after Haggerty 1976); Inter. = Intercumulus; Xeno. = Xenocrystic?

olivines (Figs. 1c and 3b) and are close in composition to alteration phases observed in NWA 817 and Lafayette, except for somewhat higher SiO_2 and, in the case of Lafayette, lower Al_2O_3 and CaO. A significant feature of alteration minerals in MIL 03346 that differs from those described in other nakhlites is the presence of modified pyrrhotites and the pervasive, localized alteration surrounding them (Fig. 8). These localized zones of alteration preserve evidence of Fe-rich pyroxene alteration, the presence of clays, and the alteration of sulfide-rich phases to hematite (Table 7) and/or magnetite, indicating that some of the large magnetites may be pseudomorphs. Unlike Nakhla, Governador Valadares, and Lafayette (Bridges and Grady 2000), goethite, siderite, gypsum, or anhydrite were not observed in the sections of MIL 03346 studied here. A single poorly formed Ba celestite was recognized in a localized zone of alteration; however, it was too small to be analyzed quantitatively.

Rare Earth and Minor Element Mineral Chemistry

Rare earth element (REE) concentrations for augite and olivine cores and rims and intercumulus glass are presented in Fig. 9 and Table 8. Augite cores in MIL 03346 have La concentrations ranging from 0.3 to 1.1 ppm and Yb concentrations from 0.38 to 0.61 ppm. The REE patterns (Fig. 9a) are comparable to those in other nakhlites, with relative depletions in La and Ce, negative slopes to the heavy REE (HREE) and negative Eu anomalies (Eu/Eu* = 0.70–0.88). The REE abundances from cores to rims of the nakhlite pyroxenes vary over an order of magnitude (Fig. 9a). Fe-rich pyroxene rims generally have higher REE abundances and more pronounced Eu anomalies (Eu/Eu* = 0.64–0.67) than the augite cores, but REE patterns are similar (Fig. 9a). Miller Range 03346 augite Cr, Sc, and V contents are comparable to the ranges measured in other nakhlites, while the Fe-rich rims

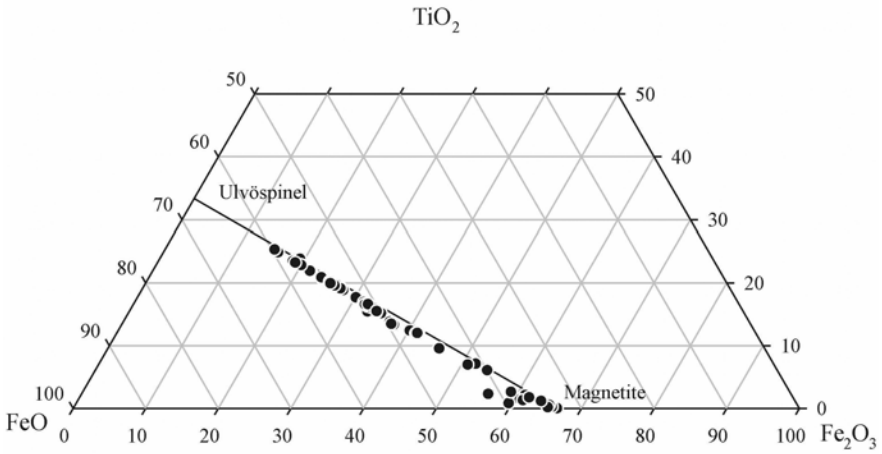

Fig. 6. FeO-Fe_2O_3-TiO_2 phase equilibria for MIL 03346 demonstrating the presence of pure magnetite in MIL 03346. No ilmenite fractions were measured.

of augites have lower concentrations of Cr and similar but more variable concentrations of V and Sc.

The olivines are relatively enriched in light REE (LREE), with abundances that are higher compared with olivines previously analyzed from nakhlites (Fig. 9b) (Nakamura et al. 1982; Wadhwa and Crozaz 1995, 2003). The REE concentrations increase towards the rims of olivines in contact with the intercumulus matrix and all olivines show depletions in Ce relative to La and Pr (Fig. 9b). Cerium anomalies and LREE enrichment in olivines from meteorites found in hot and cold deserts are typically attributed to terrestrial alteration (e.g., Crozaz et al. 2003). Nickel abundances in the olivine cores (443–667 ppm) are higher than in the Fe-rich rims (237–312 ppm). The REE patterns for MIL 03346 intercumulus glass (Fig. 9c) are LREE enriched and similar to the pattern presented for intercumulus material in Y-000593 and to an inclusion within olivine measured in NWA 998 (Wadhwa and Crozaz 2003). The vitrophyric intercumulus glasses have large ranges of Eu/Eu* (= 0.87–1.27) as well as Cr, Sc, V, Ni, P, Sr, Ba, and Zr abundances.

Whole-Rock Major and Trace Element Chemistry

Major element data for MIL 03346 are presented in Table 9. MIL 03346 has a whole rock major element composition that is broadly similar to other nakhlites but has higher Al_2O_3, TiO_2, Na_2O, K_2O, and lower MgO, which can be attributed to the proportion of intercumulus material in MIL 03346 (with the notable exception of NWA 817; Sautter et al. 2002). The major element chemistry of MIL 03346 (Mg# = 48.7) is most similar to NWA 817 (Mg# = 48.1) and is only slightly less magnesian than other nakhlites (Mg# = 49.3 to 51.6). We also present new whole rock ICP-MS data for MIL 03346 (Table 9). Due to the high modal abundance of mesostasis in MIL 03346, the whole rock elemental abundances of U, Th, and REE are elevated compared to other nakhlites, although the U/Th ratios are similar (0.25 for MIL 03346 versus 0.23–0.26 for other nakhlites). Ratios of La/Yb are variable for the nakhlites and may reflect discrepancy due to inter-laboratory bias. Nevertheless, the nakhlites are all LREE enriched (La/Yb = 4.49–7.25) with similar REE patterns (Fig. 9c). The primary difference between NWA 817 and MIL 03346 (the two best characterized nakhlites in terms of their incompatible element abundances) is that the LREE are more elevated in NWA 817, perhaps due to hot desert alteration processes. Miller Range 03346 has a lower Rb/Sr (0.036) ratio than other nakhlites (0.041–0.069) and a negative Eu anomaly (Eu/Eu* = 0.87), similar to NWA 817 and Y-000593 (Eu/Eu* = 0.90–0.91). The similarity in whole-rock compositions of the nakhlites reinforces the notion that these meteorites originated from the same or similar parental melts on Mars.

DISCUSSION

Textural and mineralogical study of MIL 03346 reveals several common features and subtle contrasts compared with the other nakhlites that may modify existing models for nakhlite petrogenesis. We discuss the evidence for a Martian origin for MIL 03346, demonstrate its classification as a nakhlite and, to facilitate comparison with other nakhlites, describe some of the salient features of the meteorite including 1) secondary alteration, 2) constraints on eruption conditions, and 3) the nature of cumulus and intercumulus material in MIL 03346 and their parental melt compositions. Ultimately, we discuss the petrogenesis of MIL 03346 and the other nakhlites based upon petrological and chemical constraints.

Nakhlite Classification and Martian Origin for MIL 03346

Miller Range 03346 shares a large number of petrological and chemical similarities with other nakhlites,

Table 6. Representative EMPA data for intercumulus matrix glass and silica-rich fractions in MIL 03346.

	Nakhla[a]	Al-rich glass				Al-poor glass		K-P-Ca-rich glass			Silica-rich zones	
wt%	Glass											
SiO_2	72.5	60.3	63.6	61.1	62.4	83.6	76.5	59.6	54.2	59.0	96.2	98.8
TiO_2	0.29	0.53	0.31	0.85	<0.03	0.65	0.18	0.55	0.66	0.91	0.11	0.10
Al_2O_3	11.1	17.1	17.6	16.8	23.3	4.9	10.9	17.0	15.3	16.3	1.19	0.75
Cr_2O_3	–	<0.05	<0.05	<0.05	<0.05	<0.05	<0.05	<0.05	<0.05	<0.05	<0.05	<0.05
MgO	0.81	0.12	0.05	0.07	<0.03	0.09	0.15	0.14	0.17	0.05	0.11	<0.03
CaO	1.52	5.31	3.94	4.81	5.07	1.21	2.28	3.71	6.05	7.03	0.15	0.08
MnO	–	0.03	0.09	0.11	<0.03	0.09	<0.03	0.05	0.19	0.09	0.08	<0.03
FeO	0.22	7.40	3.85	6.54	0.76	5.72	4.93	7.15	11.84	5.38	1.76	0.73
Na_2O	2.33	5.77	5.98	5.97	8.01	1.66	3.78	5.31	5.54	5.76	0.56	0.39
K_2O	9.60	1.04	2.63	1.79	0.87	0.36	0.80	3.33	1.56	1.38	0.03	0.04
P_2O_5	–	1.51	0.70	1.10	<0.03	0.51	0.49	0.86	2.42	2.72	<0.03	0.03
SO_2	–	0.30	1.01	0.18	<0.05	0.18	<0.05	0.13	0.39	0.12	0.08	0.12
Total	98.4	99.4	99.8	99.3	100.4	99.0	100.0	97.9	98.3	98.7	100.3	101.0
24 oxygens												
Si		8.34	8.61	8.45	8.30	10.8	9.95	8.43	7.86	8.19	11.7	11.8
Ti		0.06	0.03	0.09	0.00	0.06	0.02	0.06	0.07	0.10	0.01	0.01
Al		2.78	2.81	2.74	3.65	0.75	1.67	2.84	2.61	2.68	0.17	0.11
Cr		0.00	0.00	0.00	0.00	0.00	0.00	0.00	0.00	0.00	0.00	0.00
Mg		0.03	0.01	0.01	0.00	0.02	0.03	0.03	0.04	0.01	0.02	0.00
Ca		0.79	0.57	0.71	0.72	0.17	0.32	0.56	0.94	1.05	0.02	0.01
Mn		0.00	0.01	0.01	0.00	0.01	0.00	0.01	0.02	0.01	0.01	0.00
Fe		0.86	0.44	0.76	0.08	0.62	0.54	0.85	1.44	0.63	0.18	0.07
Na		1.54	1.57	1.60	2.07	0.42	0.95	1.46	1.56	1.55	0.13	0.09
K		0.18	0.45	0.32	0.15	0.06	0.13	0.60	0.29	0.24	0.00	0.01
P		0.18	0.08	0.13	0.00	0.06	0.05	0.10	0.30	0.32	0.00	0.00
S		0.04	0.13	0.02	0.00	0.02	0.00	0.02	0.05	0.02	0.01	0.01
Total		14.78	14.72	14.84	14.98	12.93	13.66	14.95	15.18	14.78	12.26	12.14

[a]Composition of Nakhla glass from Berkley et al. (1980).

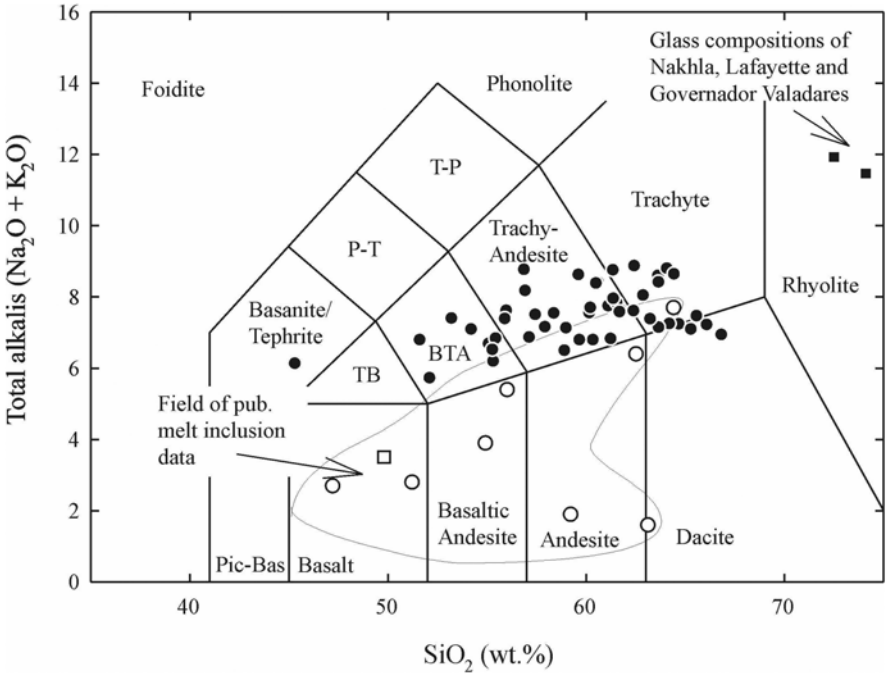

Fig. 7. Total alkali versus silica plot for vitrophyric intercumulus glass compositions in MIL 03346 (filled circles). Also plotted are melt inclusion data from Nakhla (unfilled circles and square; Longhi and Pan 1989; Harvey and McSween 1992a; Treiman 1993; Kaneda et al. 1998; Treiman and Goodrich 2001; Varela et al. 2001; Stockstill et al. 2005) and intercumulus matrix glasses from Lafayette, Governador Valadares, and Nakhla (these samples overlap on this plot) (Berkley et al. 1980). MIL 03346 glasses span a wide compositional range but are dominantly trachy-andesitic in composition.

including i) similar whole rock major and trace element compositions, ii) a similar cumulate texture with cumulus augite (Mg# = 0.64) and olivine (Mg# = ≤0.43), and variably crystallized intercumulus material, iii) Fe/Mn ratios of pyroxene and olivine that lie along the Martian Fe/Mn trend, and iv) oxygen isotope compositions that lie along the Mars mass fractionation line (M. J. Spicuzza, unpublished data) There are a number of lines of evidence to suggest that SNC meteorites originate from Mars. Several of the shergottite meteorites contain a trapped gas component that is identical (within analytical uncertainty) to the Martian atmosphere analyzed by the Viking landers on Mars (e.g., Bogard and Johnson 1983; Weins et al. 1986). In addition, the young ages of nakhlites (~1.3 Ga) suggest formation on a large, active planet other than Earth (e.g., McSween 1994). Preliminary measurements of Xe isotopes by Murty et al. (2005) have shown that Martian atmosphere-like compositions are preserved in MIL 03346, and noble gas cosmogenic exposure ages are similar to those of other nakhlites (~10–11 Ma). These lines of evidence point to Mars as the only reasonable source of MIL 03346 and the other nakhlites.

Secondary Alteration of MIL 03346 and Comparison with Other Nakhlites

Secondary alteration occurs around the large, rare cumulus olivines as red-orange weathered areas and as zones of incipient alteration around pyrrhotite in MIL 03346 resulting in the formation of hematite (Fig. 8). This process may have occurred through the release of H_2S or HS^- species at an elevated oxygen fugacity (e.g., King et al. 2004) after alteration by aqueous fluids, indicating a degree of in situ and localized alteration in MIL 03346. All of the nakhlites contain clay and iddingsite weathering products, whose origin has been attributed to the presence of brines flushing through the nakhlite parent flow (e.g., Bridges and Grady 2000; King et al. 2004). The cross-cutting relationships of cracks and fusion crusts with some of the alteration products in nakhlites have been used to suggest a preterrestrial origin (Bridges and Grady 2000; Imae et al. 2003). Therefore, the observed localized and more pervasive alteration in the nakhlites suggests hydrothermal alteration of the cooling lava in a surface or shallow crustal environment on Mars. As such, alteration of pre-existing cumulus olivine, magnetite, and pyrrhotite phases reflects the disequilibrium of these phases with the intercumulus matrix. For example, parts of the pyrrhotites that are armored by Fe-rich pyroxene do not show alteration, whereas the unarmored portions in contact with the intercumulus material have been altered to hematite (Fig. 8a). This relationship might indicate that the lava flow itself contained the volatile species (e.g., H_2O, CO_2) responsible for alteration of the pyrrhotite. As noted previously by Mikouchi et al. (2003), the degree of secondary alteration appears to be similar in all nakhlites,

Table 7. Representative EMPA data for alteration phases found in MIL 03346 versus some examples of NWA 817 and Nakhla alteration.

Host/morph	NWA 817	Olivine	Olivine	Olivine	Olivine	Pyrrhotite	Pyrrhotite	Hematite	Nakhla	Nakhla	Fe-Px
wt%	Idd. vein[b]	Idd. vein	Idd. vein	Idd. vein	Idd. vein	Altered	Altered		Siderite[c]	Goethite[c]	Alteration
SiO_2	43.6	44.9	44.9	44.6	45.5	1.64	1.61	1.54	2.15	3	10.6
TiO_2	0.03	0.05	0.05	0.06	0.04	1.40	2.72	1.92	–	–	0.09
Al_2O_3	<0.03	0.21	0.14	0.11	0.41	0.73	0.71	0.88	0.23	0.62	1.67
FeO	34.2	37.6	35.1	38.1	35.8	84.9	84.9	87.6	24.5	–	66.4
MgO	5.99	3.21	3.09	3.20	2.91	0.11	0.18	0.15	7.00	–	–
V_2O_3	–	–	–			0.07	<0.05	–	–	–	<0.05
Cr_2O_3	<0.05	0.05	0.06	<0.05	<0.05	<0.05	–	<0.05	0.15	–	0.09
SO_2	–	–	–	–	–	2.06	7.43	2.03	2.12[a]	48.8[a]	5.00
CaO	0.10	0.08	0.06	0.09	0.06	0.27	0.46	0.19	0.23	41.9	0.25
MnO	0.53	0.66	0.62	0.70	0.62	0.12	0.18	0.21	19.9	–	0.57
Na_2O	<0.03	<0.03	<0.03	<0.03	<0.03	–	<0.03	<0.03	1.65	–	<0.03
Total	84.4	86.8	84.1	86.8	85.3	91.3	98.2	94.5	55.8	–	84.7
Oxygens/Figs.		4 (Fig. 3b)	4	4	4	12	12	12 (Fig. 8)			12 (Fig. 8)

[a]As SO_3.

[b]Sautter et al. (2002).

[c]Bridges and Grady (2000).

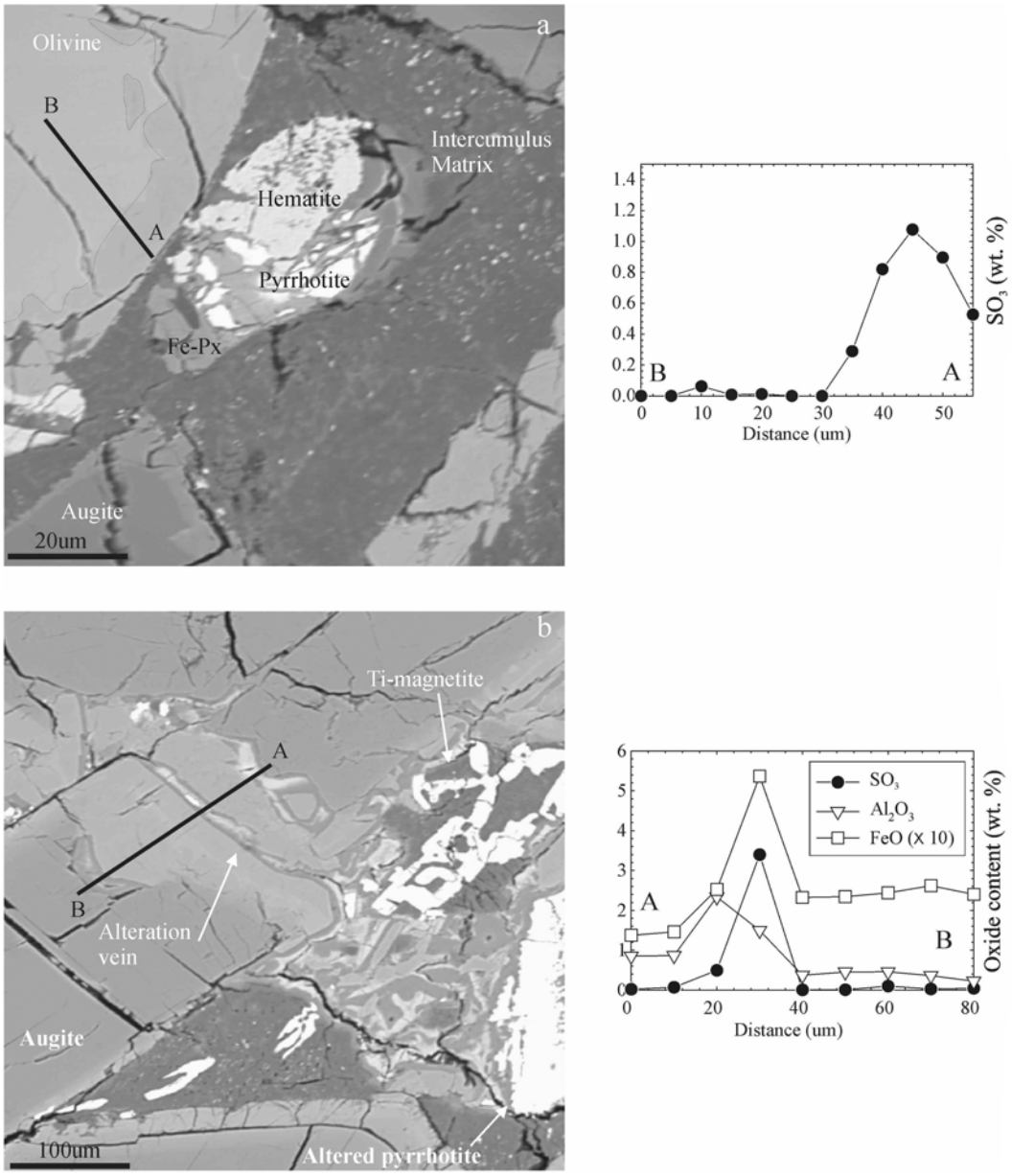

Fig. 8. BSE images of typical secondary alteration assemblages in MIL 03346 with EMPA traverses demonstrating the enrichment of S in hydrated olivine rims and in alteration veins. a) Large cumulus pyrrhotite partially armored by Fe pyroxene but locally altered to hematite and partially hydrated olivine adjacent to intercumulus matrix (thin dashed line indicates approximate hydration limit). b) Alteration zone associated with altered pyrrhotite and EMPA traverse of hydrothermally altered vein. Both EMPA traverses indicate the altered zones of the partially hydrated cumulus silicates are partially enriched in sulfur, most likely from the adjacent altered pyrrhotites.

suggesting fluid activity was uniform throughout the nakhlite body.

Crystallization Conditions for MIL 03346

Although textural analysis of the cumulus augite indicates long residence times (this study; Lentz et al. 1999), possibly in a shallow-level Martian magma chamber, the presence of glass and skeletal mineral phases and the conspicuous absence of albitic feldspar laths suggest rapid crystallization of the intercumulus matrix of MIL 03346. This feature, in conjunction with the relatively forsteritic olivine cores and the thin hedenbergite pyroxene rims surrounding cumulus augites, indicates that MIL 03346 underwent the fastest cooling of any nakhlite. Because Fe-Mg diffusion is faster in olivine than augite, the observation of more forsteritic cores in MIL 03346 is consistent with faster cooling rate estimates for this nakhlite (3–6 °C/hr) (Hammer and Rutherford 2005) relative to other nakhlites (e.g., Treiman 2005). Independent estimates of oxygen fugacity

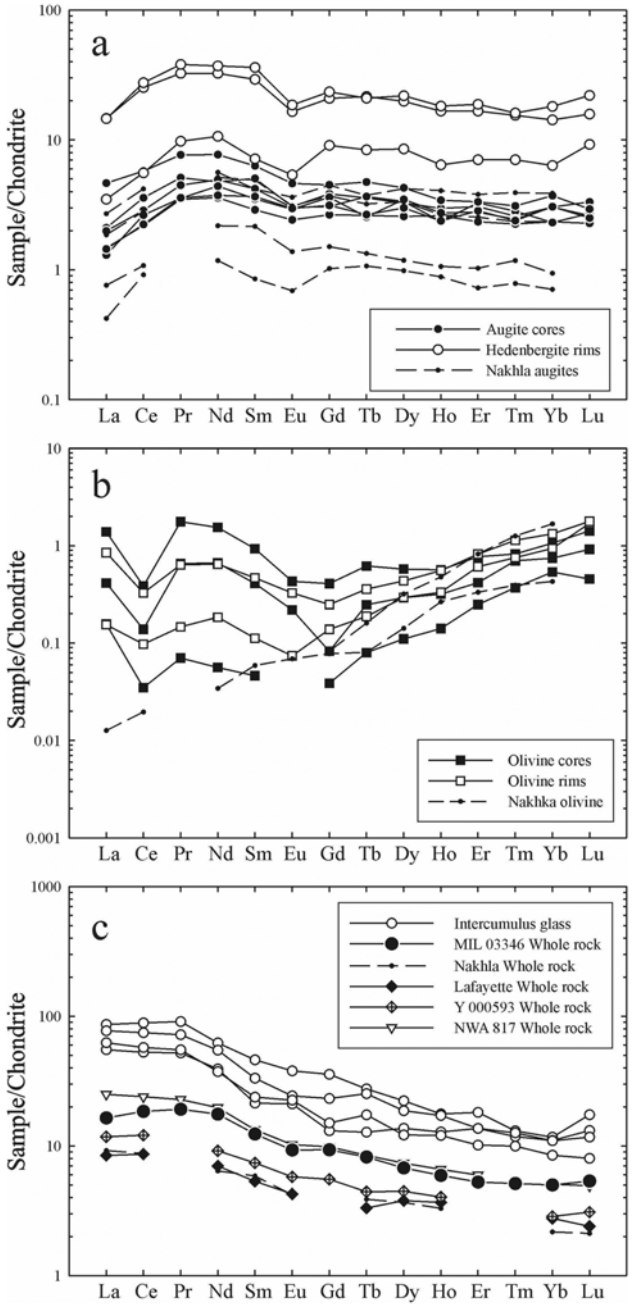

Fig. 9. Chondrite-normalized REE patterns for: a) pyroxenes, b) olivines, and c) intercumulus glasses and MIL 03346 whole rock. Data for other nakhlites are from Wadhwa and Crozaz (1995) or are listed in Table 9. MIL 03346 pyroxenes have elevated REE relative to Nakhla, while olivines in MIL 03346 are also anomalously rich in LREE with negative Ce anomalies. Nakhlite whole rock and MIL 03446 intercumulus glass REE patterns are parallel to sub-parallel. Normalization values from Anders and Grevesse (1989).

indicate an oxidation state near the NNO buffer, implying that MIL 03346 may be the most oxidized SNC meteorite recognized so far (Hammer and Rutherford 2005; Dyar et al. 2005). It is likely that cooling and crystallization of the intercumulus matrix in MIL 03346 occurred at higher oxygen activities and degrees of undercooling than for other nakhlites.

Textural constraints on crystallization conditions show that the cumulus augite population forms a clustered, poorly sorted crystal framework with partial overgrowth by hedenbergite rims. Therefore, associations of cumulus minerals that touch one another and those that abut intercumulus matrix are important because they reveal the relative order of interaction between these phases. For example, when two augite grains are in contact, no compositional gradient is observed, indicating that augite crystals were in contact prior to late overgrowth, consistent with a clustered crystal framework. There is no petrologic evidence for chemical diffusion or overgrowth acting on cumulus phases through interaction with intercumulus melts prior to the cooling event that generated the cumulate texture and glassy intercumulus matrix of MIL 03346.

There are also notable differences between the major cumulus phases in MIL 03346. In augite, the Fe-rich growth zones are only ~10 μm, whereas for the olivine the zonation can be evident to depths of up to 100 μm. Olivine probably represents a cumulus phase in the nakhlites, based on the variable contents of this mineral within different nakhlites and relatively large grain sizes that contrast with the fast cooling rates estimated for intercumulus material. Similar differences in zonation profiles have been recognized in Nakhla, Governador Valadares, and NWA 817 (e.g., Sautter et al. 2002). Diffusive sub-solidus re-equilibration between Mg-rich cores and Fe-rich rims is dramatically faster for olivine than for pyroxene (e.g., Harvey and McSween 1992b). Zoning in cumulate augite crystals does not affect the homogenous core compositions, which, therefore, must represent magmatic core compositions. For olivine, Fe-Mg diffusion took place in a marginal growth zone of ~100 μm such that the characteristic diffusion length is less than the crystal radius of the largest olivine crystal. It can be inferred that the olivine cores of MIL 03346 are the least equilibrated of all the nakhlites. Therefore, MIL 03346 replaces NWA 817 as the least equilibrated nakhlite, extending the annealing trend recognized by Harvey and McSween (1992b), from Lafayette (highly equilibrated), to Governador Valadares (partially equilibrated), to Nakhla (less equilibrated).

Determination of Nakhlite Parental Magma Compositions from MIL 03346

Overgrowth and diffusive equilibration of cumulus minerals indicate disequilibrium with the intercumulus melt in MIL 03346. Disequilibrium between cumulus and intercumulus material can occur in two main ways. It can occur through open-system processes, such that cumulus minerals formed from one melt are entrained in another melt with different physio-chemical properties. It can also occur

Table 8. Representative trace element and REE abundances in silicate minerals and glass from MIL 03346 measured by ion-microprobe.

ppm	C-3 core	C-4 core		C-1 rim		E-1 core	E-2 core		D-2 rim		Glass average	
	Olivine	Olivine	1σ	Fe-Ol	1σ	Augite	Augite	1σ	Fe-Px	1σ	Inter.	1σ
P	97.9	51.4	1.7	332.5	2.4	24.6	16.9	1.2	57.2	4.5	3980.7	16.8
Sc	8.95	8.56	0.14	9.70	0.14	65.5	63.1	0.5	83.0	0.7	4.60	0.29
V	11.7	10.3	0.2	14.4	0.2	196	192	1.1	247.1	1.4	6.9	0.3
Cr	207.9	215.2	0.9	69.1	0.6	2754	3136	5.5	214.7	1.1	4.4	0.2
Ni	624.4	647.3	5.6	237.3	3.8	320	308	15.0	528.3	29.4	79.8	8.4
Rb	1.55	0.75	0.19	1.61	0.19	0.58	1.15	0.53	0.70	0.94	24.65	1.16
Sr	0.205	0.102	0.023	0.181	0.027	25.92	23.22	0.44	26.83	0.70	661.69	2.89
Y	0.511	0.289	0.025	0.593	0.024	3.84	3.40	0.15	8.89	0.42	23.29	0.49
Zr	0.276	0.208	0.021	0.219	0.016	2.83	2.19	0.16	15.27	1.04	121.43	1.72
Ba	0.129	0.169	0.026	0.109	0.016	0.16	0.13	0.06	0.64	0.18	254.06	2.59
La	0.097	0.037	0.013	0.036	0.010	0.30	0.34	0.04	0.82	0.14	16.50	0.53
Ce	0.084	0.021	0.011	0.059	0.009	1.59	1.35	0.12	3.37	0.46	41.24	0.94
Pr	0.058	0.006	0.007	0.013	0.004	0.32	0.32	0.03	0.87	0.13	6.02	0.28
Nd	0.301	0.025	0.015	0.083	0.010	2.00	1.69	0.09	4.82	0.38	21.89	0.61
Sm	0.060	0.007	0.008	0.017	0.007	0.52	0.54	0.06	1.05	0.22	4.58	0.33
Eu	0.012	0.000	0.002	0.004	0.002	0.16	0.17	0.01	0.30	0.05	1.48	0.16
Gd	0.016	0.008	0.019	0.027	0.010	0.71	0.62	0.10	1.79	0.39	4.28	0.50
Tb	0.009	0.003	0.003	0.007	0.002	0.09	0.10	0.02	0.30	0.06	0.75	0.09
Dy	0.071	0.027	0.007	0.071	0.006	0.84	0.73	0.05	2.07	0.18	4.05	0.21
Ho	0.018	0.008	0.002	0.019	0.003	0.15	0.13	0.02	0.36	0.06	0.83	0.06
Er	0.066	0.040	0.006	0.097	0.007	0.44	0.45	0.03	1.12	0.11	2.21	0.14
Tm	0.017	0.009	0.002	0.018	0.003	0.06	0.06	0.01	0.17	0.03	0.29	0.03
Yb	0.121	0.087	0.011	0.152	0.012	0.49	0.50	0.04	1.03	0.14	1.71	0.16
Lu	0.022	0.011	0.003	0.041	0.005	0.08	0.06	0.01	0.22	0.05	0.31	0.04

Fe-Ol = Fe-rich olivine; Fe-Px = Fe-rich pyroxene; Inter. = intercumulus matrix glass average (n = 4). 1σ errors based on counting statistics.

Table 9. Major and trace element compositions of nakhlite MIL 03346 and published data for nakhlites.

Sample	MIL 03346	Nakhla	Lafayette	Gov. Valad.	Y-000593	NWA 817			
Major	EMPA[a]	XRF[b]	EMPA (FC)[c]	Wet. chem.[d]	Wet. chem.[e]	INAA[f]			
Trace	ICP-MS	INAA[g]	INAA[g]	I.D. TIMS[h]	INAA[g]	ICP-MS[f]			
wt%								St. dev. (UT-EMPA)[a]	
SiO_2	49.5	49.3	46.9	49.5	47.9	50.8		0.32	
TiO_2	0.68	0.35	0.42	0.35	0.47	0.61		0.06	
Al_2O_3	4.09	1.64	2.74	1.74	1.91	3.28		0.48	
Cr_2O_3	0.19	0.25	0.19	0.21	0.24	0.27		0.03	
MgO	9.26	11.8	12.9	10.9	11.1	10.3		0.37	
CaO	14.4	14.3	13.4	15.8	14.7	13.1		0.41	
MnO	0.46	0.55	0.5	0.67	0.59	0.53		0.03	
FeO	19.1	21.7	21.6	19.9	22.1	19.8		0.23	
Na_2O	0.96	0.57	0.4	0.82	0.64	0.94		0.19	
K_2O	0.20	0.17	0.11	0.43	0.18	0.3		0.04	
P_2O_5	0.23	0.10	0.45	–	0.29	–		0.06	
SO_3	0.06	0.02	0.04	–	0.07	–		0.03	
Total	99.2	100.8	99.7	100.3	100.2	100.0			
Mg#	48.7	49.3	51.6	51.1	50.7	48.1			
ppm							BE-N[i] Durham	St. dev.	Certified
Sc	52.4	56.1	51.1	–	58.2	47.0	22.9	0.5	22.0
V	210	–	–	–	–	181	226	5	235
Cr	1285	–	–	–	–	1519	359	4	360
Co	38.7	36.9	45.4	–	43.9	49.0	60.1	1.1	61.0
Ni	58.1	58.0	90.0	–	56.0	71.0	294.5	5.6	267.0
Cu	13.3	–	–	–	–	12.7	72.3	0.9	72.0
Zn	61.5	70.0	79.0	–	89.0	71.5	125.2	1.4	120.0
Ga	6.77	3.40	3.50	–	–	6.77	17.59	0.24	17.00
Rb	4.41	4.00	3.30	3.87	4.00	6.06	47.34	0.29	47.00
Sr	121.3	65.0	80.0	55.8	90.0	145.0	1511.4	9.0	1370
Y	8.5	–	–	–	–	9.86	30.1	0.3	30.0
Zr	21.2	–	–	–	–	29.7	271.4	2.7	265.0
Nb	3.65	–	–	–	–	4.60	118.8	1.1	100.0
Cs	0.27	0.26	0.32	–	0.36	0.25	0.72	0.02	0.80
Ba	56.9	3.46	23.00	–	–	167	1022	10	1025
La	3.89	2.18	2.00	–	2.79	5.92	81.6	0.6	82.0
Ce	11.3	5.35	5.30	–	7.41	14.7	146.4	1.0	152.0
Pr	1.78	–	–	–	–	2.11	17.95	0.17	16.90
Nd	8.04	2.93	3.20	3.39	4.19	9.02	68.67	0.86	70.00
Sm	1.83	0.87	0.79	0.76	1.10	1.97	12.09	0.14	12.00
Eu	0.52	0.24	0.24	–	0.33	0.58	3.60	0.04	3.60
Gd	1.86	–	–	–	1.10	1.96	10.25	0.14	9.00
Tb	0.30	0.14	0.12	–	0.16	0.31	1.32	0.01	1.30
Dy	1.66	0.90	0.93	–	1.10	1.81	6.32	0.03	6.29
Ho	0.32	0.18	0.20	–	0.22	0.36	1.07	0.01	1.03
Er	0.84	–	–	–	–	0.95	2.40	0.04	2.48
Tm	0.13	–	–	–	–	–	0.31	0.01	0.37
Yb	0.80	0.35	0.45	–	0.46	0.82	1.82	0.02	1.80
Lu	0.13	0.05	0.06	–	0.08	0.12	0.27	0.01	0.24
Hf	0.66	0.31	0.27	–	0.40	0.78	5.64	0.06	5.40
Ta	0.21	0.10	0.10	–	0.12	0.25	6.05	0.07	5.50
Pb	0.87	–	–	–	–	1.90	4.08	0.05	4.00
Th	0.43	0.17	0.19	–	0.23	0.60	10.69	0.15	11.00
U	0.11	0.04	0.04	–	0.06	0.14	2.40	0.03	2.40

[a]20 analyses on multiple fused beads, average standard deviation (UT-EMPA) calculated from all analyses.
[b]Dreibus et al. (1982).
[c]Boctor et al. (1976).
[d]Gomes and Keil (1980).
[e]Imae et al. (2003).
[f]Sautter et al. (2002).
[g]Dreibus et al. (2003).
[h]Shih et al. (1999).
[i]BE-N replicate analyses during ICP-MS analysis of MIL 03346, 45. Certified values from Ottley et al. 2003 and references therein.

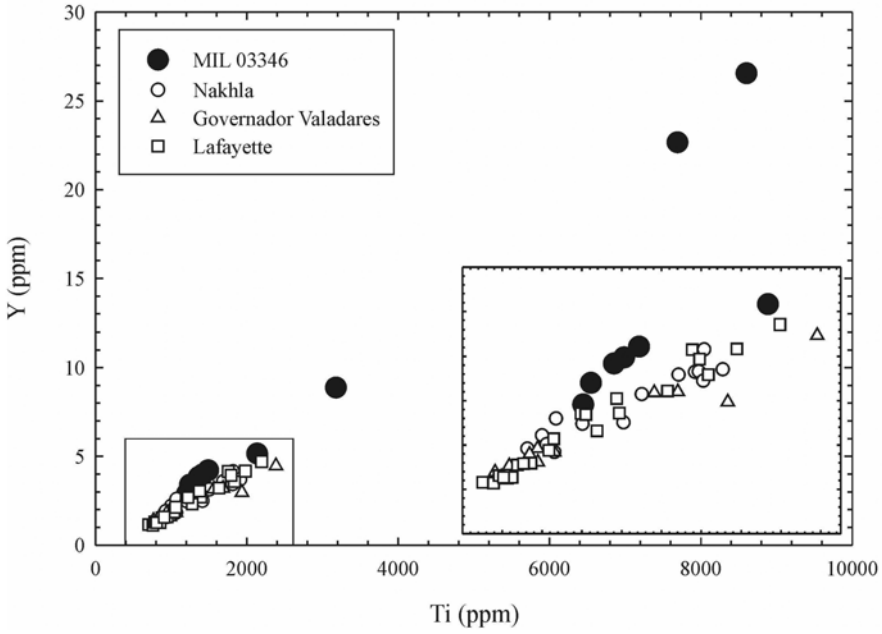

Fig. 10. Yttrium versus Ti abundances of augites and hedenbergite rims in the nakhlites. Expanded view shows MIL 03346 augite cores have elevated Y and Ti relative to other nakhlites. Data for Nakhla, Governador Valadares, and Lafayette from Wadhwa and Crozaz (1995).

through closed-system processes, such as a change in physical conditions (e.g., change in temperature, pressure, oxygen activity, or through crustal interaction with increasing fractional crystallization), resulting in a change in the equilibrium between the remaining melt and the early-formed crystals. To distinguish between these two processes, the compositions of parental magmas for MIL 03346 augite have been calculated and compared with the whole rock and intercumulus melt trace element compositions.

Because nakhlites are cumulate rocks, they are not representative of their primary magma compositions. Attempts have been made to calculate the primary magma compositions of nakhlite augite using melt inclusions. However, these studies have resulted in disparate composition estimates (e.g., Longhi and Pan 1989; Harvey and McSween 1992a; Treiman 1993; Kaneda et al. 1998; Treiman and Goodrich 2001; Varela et al. 2001; Stockstill et al. 2005). A few studies have attempted to calculate the REE compositions of nakhlite parental magmas using REE analyses of constituent mineral phases. Nakamura et al. (1982) estimated parental REE abundances by inverting REE concentrations from pyroxene separates, whereas Wadhwa and Crozaz (1995) performed REE concentration inversions using in situ ion microprobe analyses of carefully selected points within individual Nakhla augite crystals, which is the technique employed here.

Wadhwa and Crozaz (1995; 2003) demonstrated that augites in Nakhla, Governador Valadares, Lafayette, NWA 998, NWA 817, and Y-000593 preserved primary igneous zonation and that some nakhlites contain augites with more extreme trace element zonation than others. MIL 03346 has trace element zonation that spans a greater range than any previously recognized in the nakhlites (Fig 10). Excluding Fe-rich rims and assuming the most primitive cores of augites in MIL 03346 and other nakhlites have been adequately sampled, there appears to be a relative enrichment of incompatible element igneous zonation in augites. Further evidence for relative differences in initial incompatible-element inventories in nakhlites comes from similar REE abundances between an early-formed olivine inclusion from NWA 998 and late-formed intercumulus matrix in Y-000593 (Wadhwa and Crozaz 2003). MIL 03346 intercumulus matrix REE abundances are higher than those of Y-000593. Unlike Y-000593, however, MIL 03346 does not contain large phosphate mineral phases, which are strongly enriched in the REE in other nakhlites (Wadhwa and Crozaz 1995). Therefore, the extremely elevated incompatible-element abundances in Fe-rich pyroxene rims of MIL 03346 may reflect the fact that phosphates did not crystallize synchronously with them.

The REE compositions of individual augite cores in MIL 03446 can be used to estimate compositions of their parental liquids because the degree of REE equilibration between cumulus augite cores and intercumulus matrix appears to have been minimal. The first test of closed or open-system processes affecting REE abundances and ratios in MIL 03346 is to assess the level of agreement between whole rock and calculated REE patterns and abundances, which in turn can indicate closed-system crystallization of the parental melt. It is notable that the measured and calculated whole rock REE patterns and abundances are in excellent agreement (Fig. 11a). In order to model the composition of the parental melt, appropriate REE pyroxene/melt partition coefficients (*D*-values) are required. We have employed the partition

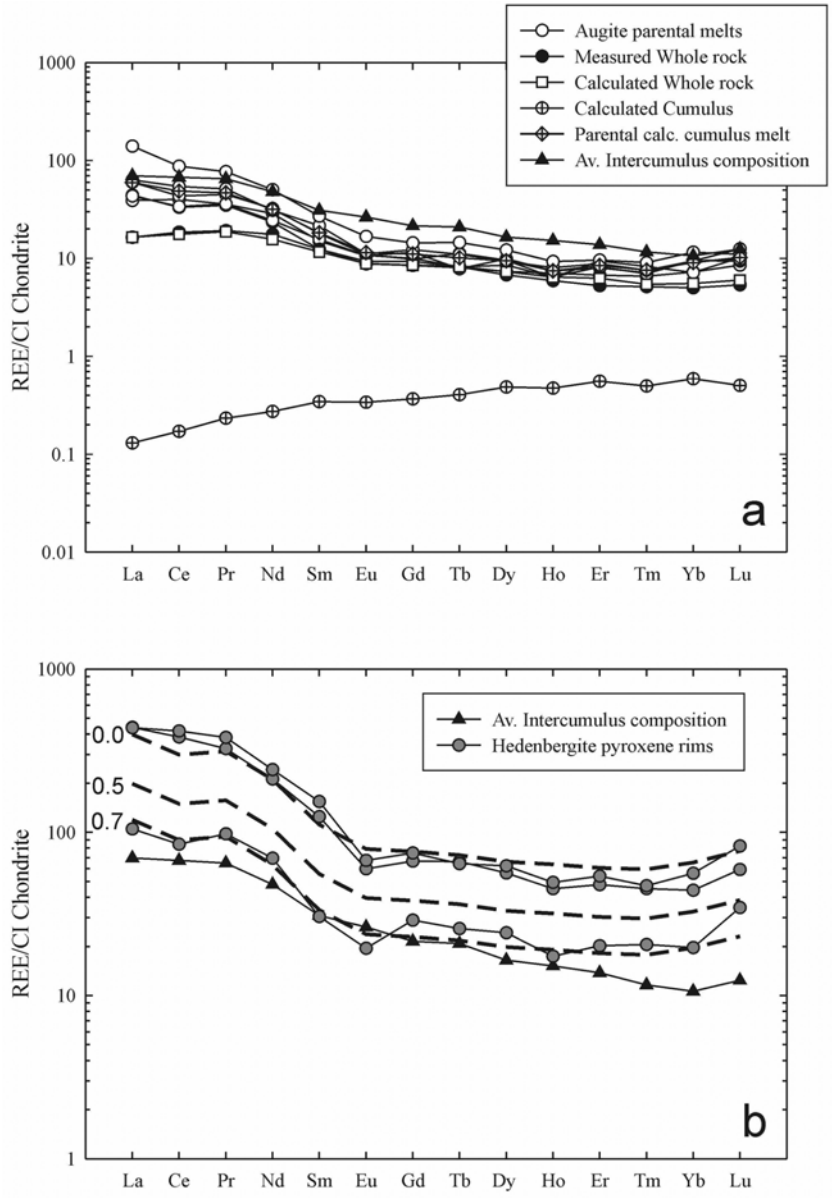

Fig. 11. a) Chondrite-normalized REE patterns of MIL 03346 whole rock and intercumulus matrix and calculated whole-rock compositions (normalization values from Anders and Grevesse, (1989). Melts in equilibrium with the cumulus component and augite cores calculated using experimental partition coefficient data of Oe et al. 2001 (see text for details). b) Fractional crystallization model (after Wadhwa and Crozaz 1995) for hedenbergite pyroxene rims and intercumulus melt. Numbers denote fraction of melt remaining (i.e., 0.7 = 30% fractional crystallization from primary melt-calculated parental melt of the lowest-REE-abundance augite core). Modeling indicates variable to late-stage fractional crystallization is responsible for the elevated REE concentrations. About 30% fractional crystallization is required to explain the intercumulus matrix REE abundances, assuming simple fractional crystallization has taken place.

coefficient data from the study of Oe et al. (2001; G. McKay, personal communication). Wadwha and Crozaz (1995) outlined the rationale for selecting similar experimental *D* values and why they are most suited to nakhlite petrogenesis. Using these *D* values, the REE abundances in the earliest formed augite (i.e., with the lowest REE concentration) in MIL 03346 have been inverted to obtain the REE composition of the parental melt in equilibrium with this core composition.

Rare earth element patterns of parental melts in equilibrium with the earliest formed augite cores in MIL 03346 are approximately parallel to the whole rock REE pattern of this meteorite (Fig. 11a). Wadhwa et al. (1995 and references therein) have demonstrated that parallelism of parent melt and whole rock REE patterns support closed-system crystallization. Additional confirmation of closed-system crystallization comes from the similar REE patterns of the intercumulus melt and the whole rock (Fig. 11a). These

results agree closely with those of other nakhlites for which similar calculations have been performed (Nakamura et al. 1982; Wadhwa and Crozaz 1995, 2003). Wadhwa and Crozaz (1995) previously demonstrated that closed-system fractional crystallization of the nakhlites can explain the composition of melts in equilibrium with late formed augite and the Fe-rich rims of augite cores and noted that additional, more complicated mechanisms are not required (e.g., Berkley et al. 1980; Treiman 1993). To test the closed-system fractional crystallization model, we performed calculations identical to those of Wadhwa and Crozaz (1995) to obtain modeled estimates of fractional crystallization for the compositions of Fe-rich augite rims in MIL 03346 (Fig 11b). Because crystallization of phosphate and plagioclase in the intercumulus matrix of MIL 03346 has not occurred to the same extent as that seen in Nakhla, direct comparison can be made between the intercumulus melt and adjacent hedenbergite rims of the cumulus augite. To do this, the REE abundances in the hedenbergite rims (e.g., with the highest REE concentration) in MIL 03346 were inverted to obtain the REE composition of the equilibrium parental melt.

Notably, despite quite different REE abundances, the overall REE patterns of equilibrium melts of hedenbergite rims and cumulus augite cores are nearly identical. Furthermore, ~30% and nearly 30–100% fractional crystallization, respectively, are required to explain the increased REE abundances in the intercumulus melt and the hedenbergite rims. Wadhwa and Crozaz (1995) found that REE abundances in Nakhla were adequately modeled by cumulus phases plus ~25% intercumulus material, consistent with the ~30% fractional crystallization estimate we calculate for the intercumulus melt in MIL 03346. Considering that cumulate phases make up ~75 to 80% of the nakhlite meteorites, there must be a missing component based on the calculated closed-system REE inventory of MIL 03346 (e.g., Fig. 11b). By summing the intercumulus matrix and the overgrowth on intercumulus augite in Nakhla, Treiman (2005) has demonstrated that the precursor intercumulus magma volume was likely to have been much greater than the observed intercumulus material preserved in nakhlites. Treiman (2005) suggested that this discrepancy could readily arise from magma metasomatism. In the next section we discuss the petrogenesis of the nakhlites and explore the possibility that the missing intercumulus melt component may in fact be the result of removal of this melt from the cumulate pile of a lava flow in an analogous way to flow differentiation on Earth.

Models for the Petrogenesis of MIL 03346 and the Nakhlites

The favored interpretation for the petrogenesis of nakhlites is that they represent cumulate igneous rocks because they are too crystal-rich and depleted in incompatible elements to represent true magma compositions (Bunch and Reid 1975). This class of model has been refined to incorporate a two-stage cooling history based on the fine-grained intercumulus matrix and cumulus augite crystals in the nakhlites (Berkley et al. 1980). Subsequent modifications have proposed that nakhlites originated as rapidly cooled lava lakes or thick lava flows based on their textural similarities to terrestrial magmatic rocks of that type (e.g., Lentz et al. 1999). The cumulate-rich igneous body model can explain the similar cosmogenic (~11 Ma) and formation ages (~1.3 Ga) of the nakhlites (e.g., Nyquist et al. 2001), their cumulate textures, and the similar chemical compositions of nakhlite whole rocks and constituent minerals. It should be noted that this model could relate to the origin of the nakhlites from a single flow or from numerous, similarly structured flows on Mars. Another class of model considers the nakhlites to be agglomerations of non-igneous mineral grains from several sources, probably chondritic materials, unrelated to Mars (Varela et al. 2001). However, the textural similarities to terrestrial basaltic cumulate rocks and the similar Fe/Mn and oxidation states of all SNC meteorites, strongly argue for petrogenesis of the nakhlites through igneous crystallization on Mars (Treiman 2005; Stockstill et al. 2005). Therefore, we place MIL 03346 within the context of a cumulate-rich igneous body on Mars.

Any model for the petrogenesis of nakhlites on Mars has to:

1. Explain the LREE-enriched nature of the nakhlites and the seemingly contrasting evidence for a long-term LREE-depleted mantle source (e.g., Shih et al. 1999).
2. Account for the cumulus phase and intercumulus matrix compositions.
3. Adequately explain the differential cooling (cumulus versus intercumulus matrix), compositional variation of olivine and pyroxene rims and the secondary alteration in the nakhlites.
4. Explain the observed modal variations of minerals and their spatial distribution patterns.
5. Be geologically realistic, despite our limited knowledge we have for the source region of the nakhlites on Mars.

Although the nakhlites are enriched in highly incompatible elements relative to moderately incompatible elements, isotopic evidence points to a mantle reservoir for the nakhlites with long-term LREE depletion (e.g., Nakamura et al. 1982; Shih et al. 1999). The nakhlites are characterized by positive ε^{143}Nd (i.e., superchondritic $^{143}Nd/^{144}Nd$), negative γ^{187}Os (i.e., subchondritic $^{187}Os/^{188}Os$), and positive ε^{182}W and ε^{142}Nd values (Treiman 2005 and references therein), consistent with partial melting from an incompatible-element-depleted and ancient mantle source that formed within the first few hundred million years of solar system evolution. The first stage in the petrogenesis of the nakhlites requires partial melting of this depleted mantle source, which was presumably rich in garnet and/or Ca-rich

pyroxene, or which had experienced some enrichment in LREE immediately prior to segregation of the nakhlite parental magma (Treiman 2005).

Textural studies of nakhlite augites reveal that they crystallized over a similar period assuming identical growth rates; by contrast, the intercumulus material within each nakhlite have different cooling histories. This relationship requires growth of the cumulus minerals in a hyperabyssal chamber or dyke-like body, prior to extrusion, consistent with cumulus olivine and augite forming at relatively low pressures (Harvey and McSween 1992b). On Earth, many phenocrystic, glomeroporphyritic, or porphyritic flows formed in continental flood basalt provinces retain geochemical evidence for storage in shallow-level magma chambers prior to eruption (e.g., Saunders et al. 1997). Therefore, a cumulate igneous model for the nakhlites must include crystallization of cumulus augite, in a shallow crustal magma body over a relatively prolonged period ($>1 \times 10^1$ yr).

We suggest that the forsteritic olivine crystallized in a shallow level magma body along with magnetite (Usp_0–Mt_{100}). The presence of large euhedral and resorbed pyrrhotites and rhombohedral magnetites in MIL 03346 may also indicate entrainment of these phases, which are only likely to be preserved in MIL 03346 because of its fast cooling rate; they have not been documented in any of the other nakhlites. In terrestrial volcanic systems, the effects of crustal assimilation, fractional crystallization, and the generation of new magma batches in the melting zone can generate a range of melt compositions that utilize the same melt pathways (e.g., Yoder 1973). In addition, mineral disequilibrium can be achieved by convective self-mixing in open-system magma chambers (Couch et al. 2001) or by entrainment of igneous crust-derived material. The recorded change in composition from the parental melt of the augite cores to the intercumulus matrix of MIL 03346 (Fig. 7) indicates that closed-system processes, similar to that of convective self-mixing, may have played an important role in the eruption of the nakhlite magma.

Fe-Mg diffusion within olivine appears to have taken place largely in situ within a cooling magma body, based on the different cooling estimates from intercumulus matrix crystallinity in the nakhlite meteorites (Fig. 12). Textural analysis shows, in addition to a lack of correlation between the cooling rates of individual nakhlites and augite crystal size, that cumulus phases formed over a substantially longer period than the cooling of a lava flow would allow. Assuming temperatures of ~1150 °C based upon the most primitive melt inclusion found in nakhlites thus far (e.g., Stockstill et al. 2005) and cooling-rate estimates for nakhlites of between ~1 and 6 °C/hr (Sautter et al. 2002; Hammer and Rutherford 2005), would mean the nakhlite body cooled over a period of 8–48 days. Using higher initial temperature estimates from Theo's flow (e.g., >1265 °C) (Lentz et al. 1999), still provides cooling histories for the nakhlites that are too short to explain the growth of the euhedral augite cumulus crystals. It is worth emphasizing that minerals formed in fast-cooled magma bodies are not euhedral but, instead, possess skeletal or hopper grain morphologies; the cumulus augites in the nakhlites do not possess these morphologies.

Extrusion and crystal settling can explain the degrees of compaction and sorting of cumulus crystals in the nakhlites (Fig. 12). An important feature of the cumulate igneous model is that nakhlites all possess clustered touching crystal frameworks with only slightly variable intercumulus "porosity." This indicates that either the flow was exceptionally crystal-rich or that a component of the flow is missing through biased sampling. Considering that cumulate phases make up ~75–80% of the nakhlite meteorites, there must be a missing component based on the calculated closed-system REE inventory of MIL 03346 (e.g., Fig.11b). This missing component may have been preserved in a shallow level magma chamber, but may also have been preserved above the cumulate pile in a lava flow on Mars. For example, terrestrial komatiites possess a lower cumulate zone ("Zone B") and an upper fast quenched, spinifex zone ("Zone A"). This same type of cumulate/upper zone relationship is also preserved in a rare example of a terrestrial flow dominated by pyroxene cumulates (Theo's Flow), which has previously been considered a close analog to the nakhlite body (Lentz et al. 1999).

Further evidence for a "missing" component for the nakhlite flows comes from the concept of a solidification front in magmas, which can distinguish the degree of crystal richness in melts. Melts that contain greater than 25% crystals are an order of magnitude more viscous than a melt free of crystals with identical physio-chemical properties, while the point of critical crystallinity (>50–55% crystals) marks a region of maximum packing generating an interlocking framework of some strength (Marsh 2002). Critical crystallinity has been reached by the nakhlites, in their current configuration (>70% crystals). Therefore, for the nakhlite magmas to have flowed, a crystal mush (<50% crystals) below the critical crystallinity point is most likely, suggesting that a substantial portion of the original parental melt may not be accounted for. If a missing upper "Zone A" komatiite-like component existed for the nakhlites, it would probably be poorly preserved after impact, because the interlocking crystal framework of the nakhlites is what provides the strength to these rocks and may have absorbed and transferred much of the energy of shock.

The quench textures and limited re-equilibration of cumulus olivine of MIL 03346 indicates a large thermal contrast between the melt and its surroundings. This might imply injection into the Martian crust as a sill or a dike, or extrusion at the Martian surface. We favor the concept of eruption and extrusion of the nakhlite magma followed by crystal settling and freezing (Fig. 12) because of the fast cooling rates and the vitrophyric textures of some nakhlites. Crystal settling is an important feature of ponded lavas on Earth (e.g., Cashman and Marsh 1988), and this appears to

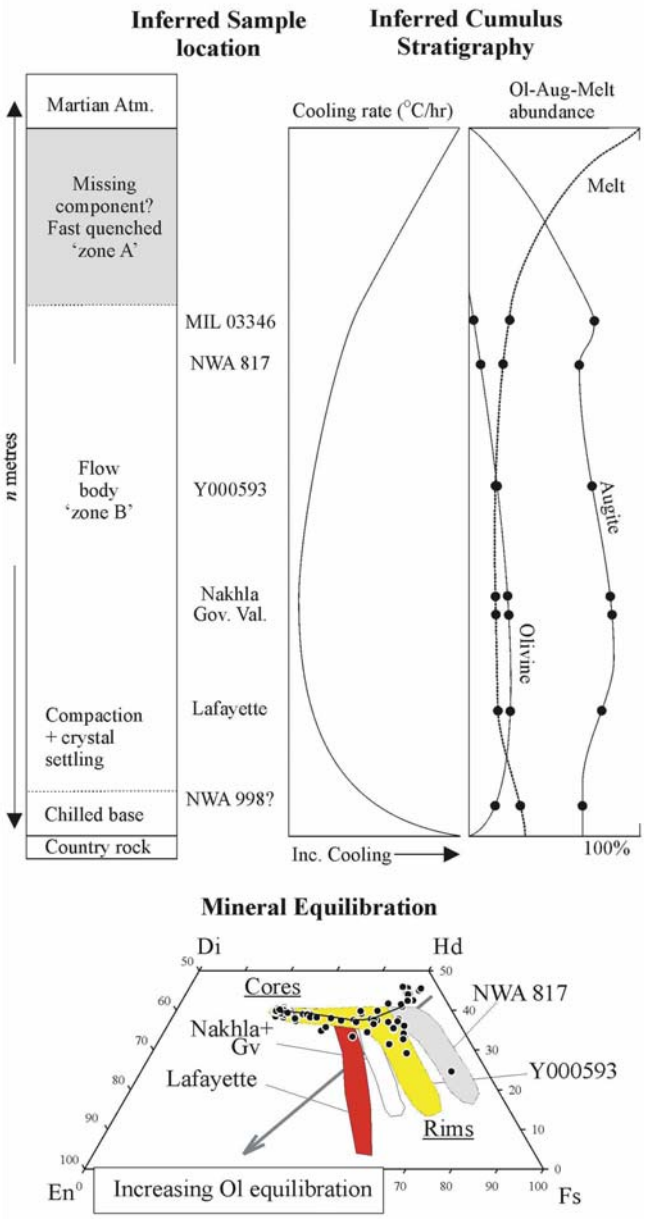

Fig. 12. Schematic model for the origin of nakhlite lava flows ~1.3 Ga on Mars. We summarize apparent variations in the putative nakhlite lava flow subsequent to crystallization of augite at shallow levels in the Martian crust. Inferred cumulus stratigraphy illustrates variation in cooling rate of intercumulus melt, modal mineralogy, and mineral compositions as a function of depth within the nakhlite flow. Mineral equilibration to varying degrees (shown by pyroxene quadrilateral and arrow for corresponding olivine equilibration) with the nakhlites corresponds to relative location within the inferred cumulus stratigraphy. We also highlight a possible missing component (percentage of total flow unknown), possibly similar to the upper zone A of komatiite flows on Earth. Succeeding these events was the impact-induced shock of nakhlites and the eventual expulsion of material into space prior to fall to Earth. Model based upon the cumulate igneous rock model of Bunch and Reid (1975); Reid and Bunch (1975); Berkley et al. (1980); Lentz et al. (1999).

have been a significant process in the petrogenesis of nakhlites (Lentz et al. 1999). In most terrestrial lava flows, olivine tends to settle out more quickly than pyroxene, resulting in more olivine-phyric lava at the base of the flow. Despite previous lack of evidence for olivine accumulation (Lentz et al. 1999), the relative lack of olivine in MIL 03346 suggests olivine crystal sorting may have taken place to some extent in the nakhlite flow. The degree of olivine equilibration, variations in pyroxene rim compositions around augite (Fig. 12) and compositions of interstitial glasses and pyroxene cores in the nakhlites, signify variable equilibration and possible pre-flow emplacement intercumulus melt heterogeneity. These observations allow a theoretical stratigraphy of an idealized nakhlite lava flow to be conceived which takes these features into account (Fig. 12).

The rationale for the placing of nakhlite samples at

relative levels (Fig. 12c) in a lava flow stratigraphy is relatively simplistic. NWA 998 is placed at the base of the stratigraphy because it possesses a crystalline intercumulus matrix and a high percentage of intercumulus materials relative to other highly equilibrated nakhlites. Such a relationship indicates limited post-emplacement removal of intercumulus melt and equilibration, consistent with a sample located at the base of a lava flow. Lafayette, as the most equilibrated nakhlite, lies below Nakhla and Governador Valadares at the center of the flow because of their slow cooling rates, high degree of equilibration with the intercumulus matrix, and very low intercumulus porosity. Y-000593 lies above Nakhla and Governador Valadares because of its slightly higher intercumulus porosity and extreme fractionation to Fe-rich pyroxene rims. NWA 817 and MIL 03346 lie close to one another on the basis of their quenched intercumulus Ti magnetite and fayalite-Ti magnetite-sulfide textures, but MIL 03346 lies closer to the top of the cumulate pile because of its higher degree of undercooling, preservation of large sulfide and oxide phases, and the high degree of Fe and Ca enrichment in augite rims.

Terrestrial flows analogous to nakhlites might include komatiitic or picro-basaltic lavas. Lentz et al. (1999) have considered Theo's flow, an Archaean ultramafic pyroxene-rich sill, to be analogous to a nakhlite lava flow. The flow thickness of the nakhlite lava would be a function of topographic constraints in the same manner as ponded flows located on Earth, or through the formation of a quenched carapace and subsequent inflation processes (e.g., Walker 1991). Estimated flow thicknesses are normally in the range of 30 m based on terrestrial flow analogs (e.g., Lentz et al. 1999). Modifications to the cumulate igneous rock model for the petrogenesis of the nakhlites presented here can explain the mineralogical and quantitative petrological features of the nakhlites.

SUMMARY

MIL 03346 represents the least equilibrated, fastest cooled Martian nakhlite discovered to date. This nakhlite contains cumulus augite, olivine, magnetite and pyrrhotite, but has a lower modal proportion of olivine than other nakhlites. Miller Range 03346 also has a vitrophyric intercumulus matrix containing skeletal Ti magnetite, reminiscent of those found in nakhlite NWA 817. Secondary alteration in MIL 03346 is restricted to zones where pre-existing pyrrhotite (i.e., pre-intercumulus matrix) has been altered and in the conchoidal fractures in the large, high Mg-olivines, indicating localized, in situ alteration of the nakhlite.

The similarity in chemical compositions of cumulus augite, modal proportions of cumulus to intercumulus materials, similar cosmic exposure and inferred crystallization ages indicates a common mode of formation for the nakhlites on Mars. This mode of formation includes:

1. Partial melting, melt extraction, and ascent of nakhlite parental magmas generated from an ancient (4.56 Ga) LREE-depleted mantle source (e.g., Shih et al. 1999).
2. Crystallization of cumulus augite, olivine (±magnetite) at shallow levels in the Martian crust.
3. Magma self-mixing and entrainment of cumulus crystals within the melt and eruption to the Martian surface.
4. Emplacement, thickening, cooling, crystal settling, overgrowth, and partial equilibration to differing extents within the nakhlite igneous body, in a manner analogous to some terrestrial mafic-ultramafic flows.
5. Secondary alteration of the nakhlite flow through hydrothermal processes, possibly immediately succeeding or even during emplacement of the nakhlite magma body on Mars at ~1.3 Ga.
6. Impact-induced release of the nakhlites from Mars' gravity, exposure in space (~10–11 Ma) and eventual collision with Earth.

Acknowledgments–We thank G. Pearson and C. Ottley for assistance with ICP-MS analysis at Durham University and A. Patchen for help with electron microprobe analyses at UT. D. Jerram, A. Mock, and D. Morgan are thanked for discussion regarding CSD and SDP analyses and for provision of the idealized crystal aspect ratio spreadsheet. Comments on an early version of this work by P. King and E. Hill and journal reviews from G. McKay, A. Treiman, N. Imae, and an anonymous referee greatly improved the quality of the manuscript. We would especially like to thank G. McKay for his thorough review and for provision of the experimental partition coefficients. This research has been supported through NASA cosmochemistry grants NAG 5-11978, NAG 5-12896, and NNG05GG03G.

Editorial Handling—Dr. Allan Treiman

REFERENCES

Alexander C. M. O'D. 1994. Trace element distributions within ordinary chondrite chondrules: Implications for chondrule formation conditions and precursors. *Geochimica et Cosmochimica Acta* 58:3451–3467.

Anders E. and Grevesse N. 1989. Abundances of the elements: Meteoritic and solar. *Geochimica et Cosmochimica Acta* 53:197–214.

Berkley J. L., Keil K., and Prinz M. 1980. Comparative petrology and origin of Governador Valadares and other nakhlites. Proceedings, 11th Lunar and Planetary Science Conference. pp. 1089–1102.

Boctor N. Z., Meyer H. A. O., and Kellerud G. 1976. The Lafayette meteorite: Petrology and opaque mineralogy. *Earth and Planetary Science Letters* 32:69–76.

Bogard D. D. and Johnson P. 1983. Martian gases in an Antarctic meteorite. *Science* 221:651–654.

Bridges J. C. and Grady M. M. 2000. Evaporite mineral assemblages in the nakhlite (Martian) meteorites. *Earth and Planetary Science Letters* 176:267–279.

Bunch T. E. and Reid A. M. 1975. The nakhlites, Part 1: Petrography and mineral chemistry. *Meteoritics* 10:303–315.

Cashman K. V. and Marsh B. D. 1988. Crystal size distribution (CSD) in rocks and the kinetics and dynamics of crystallization. *Contributions to Mineralogy and Petrology* 99:292–305.

Clayton R. N. and Mayeda T. 1996. Oxygen isotope studies of achondrites. *Geochimica et Cosmochimica Acta* 60:1999–2017.

Couch S., Sparks R. S. J., and Carroll M. R. 2001. Mineral disequilibrium in lavas explained by convective self-mixing in open magma chambers. *Nature* 411:1037–1039.

Crozaz G., Floss C., and Wadhwa M. 2003. Chemical alteration and REE mobilization in meteorites from hot and cold deserts. *Geochimica et Cosmochimica Acta* 67:4727–4741.

Dreibus G., Palme H., Rammensee W., Spettel B., Weckwerth G., and Wänke H. 1982. Composition of the Shergotty parent body: Further evidence of a two-component model for planet formation. Proceedings, 13th Lunar and Planetary Science Conference. pp. 186–187.

Dreibus G., Huisl W., Spettel B., and Haubold R. 2003. Comparison of the chemistry of Y-000593 and Y-000749 with the other nakhlites (abstract #1586). 34th Lunar and Planetary Science Conference. CD-ROM.

Dyar M. D., Pieters C. M., Hiroi T., Lane M. D., and Marchand G. J. 2005. Integrated spectroscopic results of MIL 03346 (abstract #1261). 26th Lunar and Planetary Science Conference. CD-ROM.

Floss C., James O. B., McGee J. J., and Crozaz G. 1998. Lunar ferroan anorthosite petrogenesis: clues from trace element distributions in FAN subgroups. *Geochimica et Cosmochimica Acta* 62:1255–1283.

Gomes C. B. and Keil K. 1980. *Brazilian stone meteorites*. Santa Fe: University of New Mexico Press. 159 p.

Greshake A., Stephan T., and Rost D. 2000. Combined TEM and TOF-SIMS study of exsolutions in olivine from the Martian meteorites Nakhla and Governador Valadares (abstract #1150). 31st Lunar and Planetary Science Conference. CD-ROM.

Haggerty S. E. 1976. Opaque mineral oxides in terrestrial igneous rocks. *Reviews in Mineralogy* 3:101–300.

Hammer J. E. and Rutherford M. J. 2005. Experimental crystallization of Fe-rich basalt: Application to cooling rate and oxygen fugacity of nakhlite MIL 03346 (abstract #1999). 36th Lunar and Planetary Science Conference. CD-ROM.

Harvey R. P. and McSween H.Y., Jr. 1992a. The parent magma of the nakhlite meteorites: Clues from melt inclusions. *Earth and Planetary Science Letters* 111:467–482.

Harvey R. P. and McSween H. Y., Jr. 1992b. Petrogenesis of the nakhlite meteorites: Evidence from cumulate mineral zoning. *Geochimica et Cosmochimica Acta* 56:1655–1663.

Higgins M. D. 1994. Numerical modeling of crystal shapes in thin sections: Estimation of crystal habit and true size. *American Mineralogist* 79:113–119.

Higgins M D. 2000. Measurement of crystal size distributions. *American Mineralogist* 85:1105–1116.

Hsu W. 1995. Ion microprobe studies of the petrogenesis of enstatite chondrites and eucrites. Ph.D. thesis, Washington University, St. Louis, Missouri, USA.

Imae N., Ikeda Y., Shinoda K., Kojima H., and Iwata N. 2003. Yamato nakhlites: Petrography and mineralogy. *Antarctic Meteorite Research* 16:13–33.

Irving A. J., Kuehner S. M., Rumble D., III, Carlson R. W., Hupe A. C., and Hupe G. M. 2002. Petrology and isotopic composition of orthopyroxene-bearing nakhlite NWA 998 (abstract). *Meteoritics & Planetary Science* 37:A70.

Jerram D. A., Cheadle M. J., Hunter R. H., and Elliot M.T. 1996. The spatial distribution of grains and crystals in rocks. *Contributions to Mineralogy and Petrology* 125:60–74.

Jerram D. A., Cheadle M. J., and Philpotts A. R. 2003. Quantifying the building blocks of igneous rocks: Are clustered crystal frameworks the foundation? *Journal of Petrology* 44:2033–2051.

Kaneda K., McKay G., and Le L. 1998. Synthetic nakhlite pyroxenes: A close match at last (abstract #1620). 29th Lunar and Planetary Science Conference. CD-ROM.

King P. L., Lescinsky D.T., and Nesbitt H. W. 2004. The composition and evolution of primordial solutions on Mars, with application to other planetary bodies. *Geochimica et Cosmochimica Acta* 68: 4993–5008.

Lentz R. C. F., Taylor G. J., and Treiman A. H. 1999. Formation of a Martian pyroxenite: A comparative study of the nakhlite meteorites and Theo's flow. *Meteoritics & Planetary Science* 34: 919–932.

Longhi J. and Pan V. 1989. The parent magmas of the SNC meteorites. Proceedings, 19th Lunar and Planetary Science Conference. pp. 451–464.

Marsh B. D. 1998. On the interpretation of crystal size distributions in magmatic systems. *Journal of Petrology* 39:553–599.

Marsh B. D. 2002. On bimodal differentiation by solidification front instability in basaltic magmas, part 1: Basic mechanics. *Geochimica et Cosmochimica Acta* 66:2211–2229.

McKay G. and Schwandt C. 2005. Mineralogy and petrology of a new Antarctic meteorite MIL 03346 (abstract #2351). 36th Lunar and Planetary Science Conference. CD-ROM.

McCoy T. J. and Lofgren G. E. 1999. The crystallization of Zagami shergottite: A 1 atm. experimental study (abstract). 27th Lunar and Planetary Science Conference pp. 839–840.

McSween H. Y., Jr. 1994. What we have learned about Mars from SNC meteorites. *Meteoritics* 29:757–779.

McSween H. Y., Jr. and Treiman A. H. 1998. Martian meteorites. In *Planetary materials*, edited by Papike J. J. Washington D. C.: Mineralogical Society of America. pp. 6.1–6.53.

Mikouchi T., Koizumi E., Monkawa A., Ueda Y., and Miyamoto M. 2003. Mineralogy and petrology of Yamato-000593: Comparison with other Martian nakhlite meteorites. *Antarctic Meteorite Research* 16:34–57.

Mikouchi T., Monkawa A., Koizumi E., Chokai J., and Miyamoto M. 2005. MIL 03346 nakhlite and NWA 2737 ("Diderot") Chassignite: Two new Martian cumulate rocks from hot and cold deserts (abstract #1994). 36th Lunar and Planetary Science Conference. CD-ROM.

Morgan D. and Jerram D. A. Forthcoming. On estimating crystal shape for crystal size distribution analysis. *Journal of Volcanology and Geothermal Research.*

Murty S. V. S., Mahajan R. R., Goswami J. N., and Sinha N. 2005. Noble gases and nuclear tracks in the nakhlite MIL 03346 (abstract #1280). 36th Lunar and Planetary Science Conference. CD-ROM.

Nakamura N., Unruh D., Tatsumoto M., and Hutchinson R. 1982. Origin and evolution of the Nakhla meteorite inferred from the Sm-Nd and U-Pb systematics and REE, Ba, Sr, Rb, and K abundances. *Geochimica et Cosmochimica Acta* 46:1555–1573.

Nyquist L. E., Bogard D. D., Shih C.-Y., Greshake A., Stöffler D., and Eugster O. 2001. Ages and geologic histories of Martian meteorites. *Chronology and Evolution of Mars* 96:105–164.

Oe K., McKay G., and Le L. 2001. REE and strontium partition coefficients for Nakhla pyroxenes (abstract #2174). 32nd Lunar and Planetary Science Conference. CD-ROM.

Ottley C. J., Pearson D. G., and Irvine G. J. 2003. A routine method for the dissolution of geological samples for the analysis of REE and trace elements via ICP-MS, In *Plasma source mass spectrometry: Applications and emerging technologies*, edited by Holland J. G. and Tanner S. D. London: Royal Society of Chemistry. pp. 221–230.

Prior G. T. 1912. The meteorite stones of El Nakhla El Baharia (Egypt). *Mineralogical Magazine* 16:274–281.

Reid A. M. and Bunch T. E. 1975. The nakhlites, Part II: Where, when and how. *Meteoritics* 10:317–324.

Saunders A. D., Fitton J. G., Kerr A. C., Norry M. J., and Kent R.W. 1997. The North Atlantic Igneous Province. In *Large igneous provinces: Continental, oceanic and planetary flood volcanism,* edited by Mahoney J. J. and Coffine. Washington, D. C.: American Geophysical Union. pp. 45–93.

Sautter V., Barrat J. A., Jambon A., Lorand J. P., Gillet P. H., Javoy M., Joron J. L., and Lesbourd M. 2002. A new Martian meteorite from Morocco: The nakhlite Northwest Africa 817. *Earth and Planetary Science Letters* 195:223–238.

Shih C.-Y., Nyquist L. E., and Wiesmann H. 1999. Samarium-neodymium and rubidium-strontium systematics of nakhlite Governador Valadares. *Meteoritics & Planetary Science* 34:647–655.

Stockstill K. R., McSween H. Y., Jr., and Bodnar R. J. 2005. Melt inclusions in augite of the Nakhla Martian meteorite: Evidence for basaltic parental melt. *Meteoritics & Planetary Science* 40: 377–398.

Stopar J. D., Lawrence S. J., Lentz R. C. F., and Taylor G. J. 2005. Preliminary analysis of the nakhlite MIL 03346 with a focus on secondary alteration (abstract #1547). 36th Lunar and Planetary Science Conference. CD-ROM.

Taylor L. A., Patchen A., Taylor D. H. S., Chambers J. G., and McKay D. S. 1996. X-ray digital imaging petrography of lunar mare soils: Modal analysis of minerals and glasses. *Icarus* 124: 500–512.

Treiman A. H. 1993. The parental magma of the Nakhla (SNC) achondrite inferred from magmatic inclusions. *Geochimica et Cosmochimica Acta* 57:4753–4767.

Treiman A. H. 2005. The nakhlite meteorites: Augite-rich igneous rocks from Mars. *Chemie der Erde* 65:203–270.

Treiman A. H. and Goodrich C. A. 2001. A parent magma for the Nakhla Martian meteorite: Reconciliation of estimates from 1-bar experiments, magmatic inclusions in olivine and magmatic inclusions in augite (abstract #1107). 32nd Lunar and Planetary Science Conference. CD-ROM.

Varela M. E., Kurat G., and Clocchiatti R. 2001. Glass-bearing inclusions in Nakhla (SNC meteorite) augite: Heterogeneously trapped phases. *Contributions to Mineralogy and Petrology* 71: 155–172.

Wadwha M. and Crozaz G. 1995. Trace and minor elements in minerals of nakhlites and Chassigny: Clues to their petrogenesis. *Geochimica et Cosmochimica Acta* 59:3629–3645.

Wadwha M. and Crozaz G. 2003. Trace element geochemistry of new nakhlites from the Antarctic and the Saharan deserts: Further constraints on nakhlite petrogenesis on Mars (abstract #2075). 34th Lunar and Planetary Science Conference. CD-ROM.

Walker G. P. L. 1991. Structure and origin by injection of lava under surface crust, of tumuli, “lava rises,” “lava-rise pits,” and “lava inflation clefts” in Hawaii. *Bulletin of Volcanology* 53:546–558.

Weins R. C., Becker R. H., and Pepin R. O. 1986. The case for Martian origin of the shergottites: Trapped and indigenous components in EETA79001 glass. *Earth and Planetary Science Letters* 77: 1439–1458.

Yoder H. S., Jr. 1973. Contemporaneous basaltic and rhyolitic magmas. *American Mineralogist* 58:152–171.

Zinner E. and Crozaz G. 1986a. A method for the quantitative measurement of rare earth elements by ion microprobe. *International Journal of Mass Spectrometry and Ion Processes* 69:17–38.

Zinner E. and Crozaz G. 1986b. Ion probe determination of the abundances of all the rare earth elements in single mineral grains. In *Secondary ion mass spectrometry, SIMS V,* edited by Benninghoven A., Colton R. J., Simons D. S., and Werner H. W. New York: Springer-Verlag. pp. 444–446.